



Marine and continental stratocumulus cloud microphysical properties obtained from routine ARM Cimel sunphotometer observations

Kaiden Sookdar¹, Scott E. Giangrande², John Rausch², Lihong Ma², Meng Wang², Dié Wang², Michael P. Jensen², Ching-Shu Hung³, and J. Christine Chiu³

¹Earth and Atmospheric Sciences Department, Cornell University, Ithaca, NY, USA

²Environmental Science and Technologies Department, Brookhaven National Laboratory, Upton, NY, USA

³Department of Atmospheric Science, Colorado State University, Fort Collins, CO 80523, USA

Correspondence: Scott E. Giangrande (sgrande@bnl.gov)

Received: 13 February 2025 – Discussion started: 31 March 2025

Revised: 14 August 2025 – Accepted: 2 September 2025 – Published: 6 November 2025

Abstract. This study investigates marine and continental stratocumulus (Sc) cloud properties obtained from an automated implementation of a multispectral photometer retrieval. Photometer methods simultaneously retrieve cloud optical depth (τ) and cloud droplet effective radius (r_e), with estimates for liquid water path (LWP) calculated on the availability of those quantities. These applied methods evaluate retrieved cloud properties for Sc identified during a recent 6 year period over the U.S. Department of Energy Atmospheric Radiation Measurement (ARM) program sites in Oklahoma, USA (SGP) and in the Azores, Portugal (ENA).

Modest agreement in key quantity retrievals is found between the routine photometer products and multisensor collocated profiling references. Cumulative breakdowns contingent on cloud thickness indicate increases in all retrieved quantities in thicker clouds, with larger discrepancies in the relative performance between the retrievals collected in the presence of drizzle. Under continental cloud conditions, the clouds of a similar thickness and r_e to those sampled under marine conditions report a factor of 1.5 larger τ and LWP. An $r^2 \cong 0.65$ is found between photometer τ retrievals and shadowband radiometer measurements, with photometer retrievals reporting a high (relative) bias. The τ intercomparisons indicate that variability between retrievals is a factor of three larger than errors reported from individual retrieval input perturbation tests. Photometer r_e retrievals suggest a low r^2 (< 0.1) having a standard deviation $\cong 3 \mu\text{m}$ when compared to ARM baseline multi-sensor radar/radiometer

references (accounting for offsets in the cloud droplet number concentration assumptions of the latter). However, photometer LWP calculations remain relatively unbiased in non-drizzling conditions, with errors $O(50 \text{ g m}^{-2})$ and $r^2 \cong 0.5$ to collocated radiometer and interferometer references. Additional sensitivity tests for island influences on marine Sc properties suggest that while island-influenced winds may promote larger cloud LWP or thickness, the influence could be within retrieval method uncertainty and/or collocated instrument variability.

1 Introduction

A primary source of uncertainty in Earth system model (ESM) predictions of climate change is in the representation of cloud processes and associated cloud feedback (e.g., IPCC, 2013). Several fundamental cloud properties critical to the understanding of aerosol-cloud interactions are poorly constrained by observations, with key deficiencies in our observations of cloud and precipitation droplet sizes and cloud optical depth. Observations of these cloud properties are often challenging to estimate from remote-sensing platforms and costly to obtain from in situ aircraft – requiring extensive instrument calibration, conditioning, and computational methods to retrieve the desired quantities. Nevertheless, advancing cloud observations and techniques is critical to an improved understanding of cloud formation, dis-

sipitation, aerosol-drizzle interaction, radiative impacts, and related model process studies (e.g., Albrecht, 1989; McComiskey et al., 2009). The observations of boundary layer clouds, and improved knowledge of stratocumulus cloud (Sc) processes and properties, are especially important to this ESM advancement. This is because these clouds have extensive coverage and exert controls on boundary layer dynamics and the global radiative energy balance (e.g., Klein, 1997; Bony and Dufresne, 2005; Hartmann et al., 1992; Klein and Hartmann, 1993; Wood et al., 2015; Sherwood et al., 2020). Understanding methods for retrieving Sc cloud properties is essential, as small changes in Sc coverage, thickness and cloud droplet properties can impart significant net radiative changes (e.g., Hartmann et al., 1992; Wood and Hartmann, 2006; Wood et al., 2015).

Several instruments apply different methods to simultaneously retrieve information on the cloud droplet sizes, cloud optical depth, and/or liquid water path (LWP). One such capable instrument is a multispectral photometer. The U.S. Department of Energy (DOE) Atmospheric Radiation Measurement (ARM) user facility has deployed photometers at its fixed and mobile facility deployments for over 2 decades (e.g., Gregory, 2011; Mather and Voyles, 2013; Miller et al., 2016). As a narrow field of view (FOV, 1.2°) instrument, one advantage of this instrument is in its viability for sampling a range of broken to overcast cloud cover conditions. Originally designed to retrieve aerosol optical properties, it was suggested by Marshak et al. (2004) and later expanded by Chiu et al. (2006, 2010, 2012) that the NASA AEROSOL RObotic NETwork (AERONET; Holben et al., 1998) implement a “cloud mode” strategy for its multispectral photometers. This mode is performed using two-channel radiance measurements during instrument sequences where clouds completely block the sun. When operated in this fashion, the mode enables estimates of the cloud optical depth (τ). Recently, ARM upgraded its photometers to a three-channel (440, 870, and 1640 nm wavelength) configuration to further constrain retrievals that simultaneously capture τ and cloud particle effective radius (Chiu et al., 2012). While previous two-channel (440, 870 nm) methods were applicable over vegetated land surfaces, this third channel constraint enables retrievals over ocean and ice surfaces, suitable for a range of higher-latitude and shipborne deployments (e.g., Wood et al., 2015; Lubin et al., 2020; McFarquhar et al., 2021; Wang et al., 2022; Geerts et al., 2022).

A motivation for this study is to evaluate advancements in cloud products derived from photometer measurements that are now being implemented on a routine basis in support of cloud process studies and validation for satellite, aircraft, and related retrieval applications (e.g., Minnis et al., 2011; Zhao et al., 2012; Bennartz and Rausch, 2017; Yang et al., 2018; Zhu et al., 2022). Our efforts draw on the extended ARM measurement record with a goal to deliver photometer-retrieved quantities of cloud properties as a baseline, continuing operational product. Overcast warm boundary layer

cloud conditions were targeted since we have greater confidence in retrievals of their properties as compared to mixed-phase, ice, or broken cloud conditions (Sect. 2). Stratocumulus conditions are common over ARM’s Eastern North Atlantic (ENA, Mathers and Voyles, 2013; Wood et al., 2015; Wang et al., 2022) site, while overcast low clouds are also frequent at ARM’s Southern Great Plains (SGP, Sisterson et al., 2016) site; these sites serve as our initial testbeds. Performance is explored for the photometer cloud retrieval quantities – the τ and the cloud droplet effective radius (r_e) – and a LWP estimated from those quantities. Results, discussions and physical interpretations for these product comparisons are offered in Sects. 3 and 4 for SGP and ENA, respectively. Our results compile observations drawn from a 6 year period at both sites spanning datasets collected in 2014 through 2019. Methods to track uncertainty (i.e., constrained input perturbations, wavelength-contingent variability in radiance measurements and surface albedo) have been used to partially address uncertainty quantification. We conclude with key outcomes from this study in Sect. 5.

2 Data and Methods

Datasets were collected by the U.S. DOE ARM user facility at its Southern Great Plains (SGP) site in Lamont, Oklahoma (36.607° N, 97.487° W), and its Eastern North Atlantic (ENA) facility at Graciosa Island (39.091° N, 28.025° W) in the Azores archipelago. We consider datasets from SGP and ENA for a 6 year window (Sect. 2.2). To target Sc events, these data were filtered according to a simple classification procedure and the availability of collocated reference instruments (Sect. 2.1). All retrievals have been averaged to a common 5 min sampling window, based on the collection sequence timing of the photometer. In Fig. 1, we provide an example time-height display for baseline cloud observations and photometer τ retrievals from a qualifying event over the ENA site (10 September 2017). This figure helps to illustrate some of the temporal and spatial sampling considerations when aligning these photometer retrievals with other collocated retrievals.

2.1 Stratocumulus Cloud Designation and Dataset Climatology

Stratocumulus conditions were selected based on a series of dataset availability and cloud property checks. First, we identify “events” where collocated Multifilter Rotating Shadowband Radiometer (MFRSR) observations were available, as required for τ retrieval comparisons (e.g., Min and Harrison, 1996; Min et al., 2003). Since ARM does not produce its MFRSR τ retrievals unless there are locally overcast conditions (the product defines this as 90 % cloud cover from an effective 160° FOV, inferred from downwelling shortwave irradiances, e.g., Long et al., 2006), MFRSR retrieval availabil-

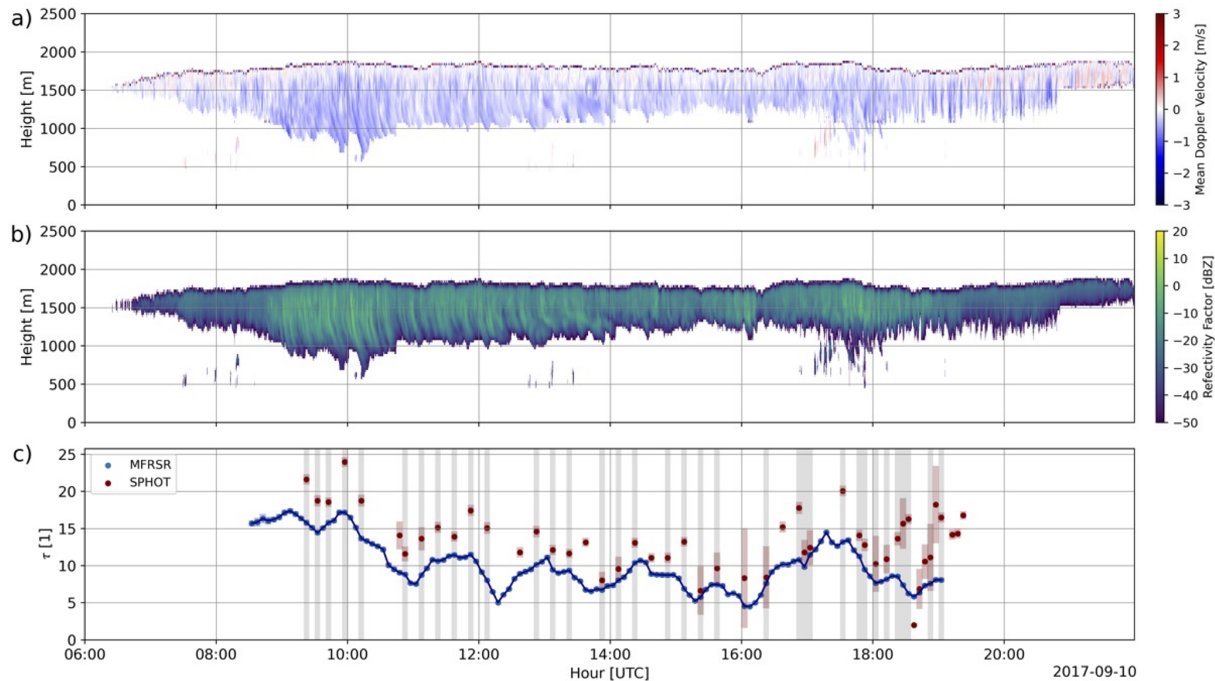


Figure 1. The KAZR (a) mean Doppler velocity and (b) radar reflectivity factor for the 10 September 2017 event at ENA. (c) Cloud optical depth τ retrievals from the photometer (SPHOT, red) and radiometer (MFRSR, blue), with shaded (grey) regions indicating cloud samples used in comparisons for this study. Instantaneous retrieval uncertainty ranges for the SPHOT follows Chiu et al. (2012), whereas MFRSR uncertainty follows Min and Harrison (1996).

ity serves as an initial check for overcast conditions. These conditions should maximize agreement between photometer and MFRSR, as broken cloud conditions may increase three-dimensional cloud-heterogeneity ambiguities on these retrievals (e.g., Turner et al., 2004; Masuda et al., 2019).

Our Sc cloud criteria loosely follow previously published classification studies and guidelines (e.g., Remillard et al., 2012). To ensure appropriate samples from widespread Sc conditions, we required each event to contain a minimum of one hour of overlapping observations from the MFRSR and photometer. The MFRSR and photometer retrievals were only available during daytime hours, which also limited the times where these overlapping overcast cloud conditions were sampled. To designate “warm/low” Sc conditions, we applied additional filters based on collocated ARM profiling products. First, the multi-sensor Active Remote Sensing of Clouds (ARSCL) product was used to estimate cloud boundaries and other radar quantities at 4 s time and 30 m height intervals using a multi-sensor approach (e.g., Clothiaux et al., 2000). The warm/low boundary layer criteria were partially enforced by only considering clouds with mean cloud echo top heights (CTH) as estimated by ARSCL below 4 km a.g.l. (above ground level), with no higher cloud layers also observed above that altitude). Second, ARM’s linearly interpolated sounding product (e.g., Fairless et al., 2021) was also used to remove events where these same ARSCL cloud layers extended above the melting level. The resulting set

of events can most often be characterized as single-layer Sc cloud decks, with our findings not significantly altered when multi-layer clouds were present.

This study did not consider samples that were associated with measurable surface precipitation. To help remove surface rain conditions or problematic comparisons therein, the mean cloud base designated by ARSCL must exceed 0.5 km a.g.l. during the intervals, while surface rain gauge and downward Ka-band ARM Zenith Radar (KAZR, e.g., Kollias et al., 2020) mean Doppler velocity in the lowest 300 m exceeding 4 m s^{-1} were also used to identify rain at/near the surface. Still, our criteria allow for Sc with in-cloud drizzle, virga and/or subcloud precipitation (i.e., sampling the presence of radar reflectivity echoes below ARSCL cloud base). This study includes retrieved LWP properties during subcloud precipitating conditions, as these comparisons may be informative on the variability between these retrievals for extended cloud and precipitation efforts. However, while in-cloud and subcloud precipitation may impact radiometric quantities, our sampling choices excluded observations under conditions with precipitation measurable by surface rain gauges, since the dome of the radiometer would become wet, implying these measurements may be further contaminated and less reliable. We also ignored any samples for which any of the instruments retrieved $\text{LWP} > 400 \text{ g m}^{-2}$, as our own visual inspection suggested such larger values typically occurred near rainy conditions. Nevertheless, in-

struments may still be influenced by water from prior precipitation that reached the sensor and was not fully shed or evaporated by a later sample time (e.g., Deng et al., 2025).

In total, our dataset contains 36 qualifying events over the SGP site, and 80 qualifying events over the ENA site. There were 855 (SGP) and 1341 (ENA) 5 min observations that met our Sc criteria. Qualifying events at the SGP site were typically associated with post-frontal stratocumulus conditions (e.g., Kollias and Albrecht, 2000; Mechem et al., 2010). These events were collected during the spring and fall seasons where frontal intrusions at SGP are most common (approx. 90 % of our dataset). A wider seasonal cloud distribution was collected at ENA, with the summertime months (June through August) being the most common for observations (approx. 35 %). The fewest Sc events were collected between December and February (approx. 15 %). This seasonal bias was expected given our focus on warm Sc conditions having CTHs below the melting level. For ENA, the dataset mean CTH was 1583 ± 375 m (suitably below the imposed 4 km top), while SGP post-frontal CTHs were slightly higher and more variable, 1827 ± 782 m.

2.2 Cimel Sunphotometer and its Automated Cloud Property Retrievals

The Cimel sunphotometer is a ground-based scanning photometer for passive remote sensing of the atmosphere, with NASA AERONET calibrating and maintaining these instruments, while processing certain data as part of their global archive. The ARM user facility deploys its photometers at three fixed sites and offers mobile deployments on request. The photometer “cloud mode” has been employed by ARM since 2007. During this mode, the instrument points to zenith and obtains high gain sky mode observations of radiance in at least 6 of its 9 channels: 380 (newer CE318T models), 440, 500, 675, 870, 1020, and 1640 nm wavelengths. Although the instrument requires less than 5 min to cycle through these channels, the availability for scheduling “cloud mode” retrievals is limited by the overall photometer sequencing and contingent on the solar zenith angle and instrument model. For much of this data record, retrievals were performed at 15 min intervals (prior to October 2017 at SGP, February 2021 at ENA) when environmental conditions allowed, while new models improved availability to 5 min updates when not operating in any of the other observing modes.

The automated retrievals we implement use zenith radiance measurements at 440, 870, and 1640 nm wavelengths. This approach simultaneously retrieves τ and r_e , with these quantities used to compute LWP as:

$$\text{LWP} = \frac{2}{3} \rho_w \tau r_e \quad [\text{g m}^{-2}], \quad (1)$$

where ρ_w is the density of water (10^6 g m^{-3}) for r_e in [m], τ is unitless, and the expression in Eq. (1) assumes that liquid water content is constant in the vertical (Stephens, 1978). The

inputs to the algorithm are the calibrated photometer zenith radiance measurements and surface albedo estimated from the Terra and Aqua Moderate Resolution Imaging Spectroradiometer (MODIS, “MCD43A2” and “MCD43A3” products, e.g., Schaaf et al., 2002). While this algorithm has been documented by Chiu et al. (2010, 2012), aspects for its implementation are briefly summarized below.

The ground-based zenith radiance for clouds at a given wavelength may be expressed as functions of the incoming radiance, the cloud r_e and τ , and the albedo of the underlying surface. By including the 1640 nm water-absorbing wavelength, Chiu et al. (2012) three-channel constraint methods enabled r_e estimates since the zenith radiance behavior for 1640 nm decreases with droplet size due to absorption, whereas radiances at 870 nm increase due to forward scattering. In practice, retrieval sensitivity of zenith radiance measurements to larger droplet size, as well as other practical limitations for radiance and surface albedo estimates, may undermine the usefulness of this third channel for r_e retrievals. To mitigate the diminishing nature of those effects, Chiu et al. (2012) implemented a multi-step perturbation approach to assess retrieval uncertainty. This approach first considers a 5 %–10 % uncertainty (normally distributed, input sensitivity) in zenith radiance and surface albedo measurements. The perturbed zenith radiances are subsequently compared to a calculated look-up table computed from the discrete-ordinate-method radiative transfer model (DISORT; Stamnes et al., 1988) over input ranges typical for ARM sites (e.g., Zhao et al., 2012, 2014). Our look-up tables were generated using an assumed gamma cloud droplet distribution with a shape parameter of 7 that aligns with Sc observations (e.g., Pörtge et al., 2023).

This implementation follows Chiu et al. (2012) by defining a solution from the photometer retrieval as “viable” when the zenith radiances agree with the look-up table to within 10 % at the 440, 870 nm wavelengths. Any viable solutions are sorted based on errors in the zenith radiance at the 1640 nm, with the five best solutions (i.e., smallest errors) averaged to generate a single solution for the set of the perturbed zenith radiance and surface albedos. Chiu et al. (2012) recommended this procedure be repeated 40 times using randomly generated perturbations. Reported retrievals for τ and r_e are obtained by taking the mean of 40 repetitions. Sensitivity tests (not shown) that considered additional perturbations did not produce significant changes in the retrieved quantities.

This perturbation uncertainty (defined here as calculating the standard error) is reported by these photometer retrievals (herein, SPHOT) as its instantaneous retrieval uncertainty. For our dataset, the average values for these reported uncertainties at ENA in τ and r_e estimates are 1.19 (unitless) and $2.1 \mu\text{m}$, respectively. For the SGP dataset, these uncertainties are 1.56 (unitless) for τ and $1.46 \mu\text{m}$ for r_e . These values may also be reported as relative errors at a level of 5 %–10 % of the reported τ estimates, or 15 %–20 % of the reported r_e estimates.

2.3 Additional ARM Cloud Property Retrieval VAPs

Comparisons are performed against related ARM products common to both sites. The primary comparison is with the MFRSR products that apply an iterative approach to compute τ and estimates r_e using an independent LWP estimate. The reported instantaneous retrieval errors for these MFRSR products are on the order of 5 % and 25 % for τ and r_e , respectively (e.g., Min and Harrison, 1996; Min et al., 2003). These products require an LWP estimate, and this LWP estimate is taken from the ARM Microwave Radiometers (MWR, 3.5° (3-channel)–5.9° (2-channel) FOV, Morris, 2019; Cadeddu, 2021). Herein, we refer to MWR retrievals for LWP according to the ARM naming “MWRRET” (e.g., Turner et al., 2007), which is a product available at a 20 s time resolution. If an LWP estimate is unavailable from MWRRET, the MFRSR retrievals assume a fixed r_e value ($r_e = 10 \mu\text{m}$), and the associated product returns only a value for τ (Turner et al., 2004). This study avoids null instances and only compares retrieved quantities in cases where non-zero LWP estimates are available. LWP estimates obtained from the MWR in previous marine studies are typically reported with uncertainties $O(10\text{--}20 \text{ g m}^{-2})$ (e.g., Cadeddu et al., 2023). These MWRRET retrievals assume all its liquid media is in the Rayleigh scattering regime. It has been found this approach overestimates LWP retrievals ($> 10\%$) at ENA in the presence of larger drizzle hydrometeors when LWP exceeds $100\text{--}200 \text{ g m}^{-2}$ (e.g., Cadeddu et al., 2023). For a secondary LWP reference, we consider LWP estimates from the Tropospheric Remotely Observed Profiling via Optimal Estimation approach (TROPOe, Turner and Löhnert, 2014, 2021; Turner and Blumberg, 2019) that were selectively available at both sites starting in 2016. These methods use atmospheric emitted radiance interferometer and MWR observations simultaneously and assume single-layer clouds. The infrared IR contributions to the TROPOe approach should dominate the solutions for LWP less than 80 g m^{-2} , with the IR saturating around 60 g m^{-2} (e.g., Turner, 2007).

The “baseline ARM retrieval of cloud microphysical properties” product (herein, “MICROBASE”, e.g., Dunn et al., 2011; Zhao et al., 2012; Huang et al., 2012) was also available to evaluate relative r_e retrieval performance. The MICROBASE algorithm uses cloud radar reflectivity Z estimates from the KAZR, along with LWP estimates from the MWR and temperature profiles from soundings. From these inputs, MICROBASE estimates the profiles for the liquid water content (LWC) and liquid r_e if the estimated LWP is positive/non-zero. The retrieved LWC follows Liao and Sassen (1994), as:

$$\text{LWC} = \left[\frac{N_0 Z}{3.6} \right]^{5/9} \text{ [g m}^{-3}\text{]}, \quad (2)$$

where N_0 is a constant reference cloud number concentration = 100 cm^{-3} , Z is the equivalent radar reflectivity factor Z (for KAZR, at 35 GHz) in linear $[\text{mm}^6 \text{ m}^{-3}]$ units.

The LWC is scaled by the ratio of the estimated LWP (from the integration of the LWC in the column) and the LWP retrieved from the MWR. Owing to this scaling, the magnitude of radar Z in Eq. (2) and/or relative calibration offsets do not strongly influence these retrievals. Thus, Z measurements only influence the relative placement of discrete LWC estimates throughout cloudy regions of any column. The authors did not directly modify this assumed fit in Eq. (2), as changes may subtly shift LWC and thus r_e values within any column, but this only weakly impacts our eventual r_e comparisons owing to the spatial and temporal averaging we employ.

The MICROBASE effective radius estimates follow Frisch et al. (1995):

$$r_e = \frac{e^{2.5\sigma^2}}{\left[\frac{4}{3}\pi\rho_w N \text{LWC} e^{9\sigma^2/2} \right]^{1/3}} \text{ [\mu m]}, \quad (3)$$

where N is a constant cloud particle number concentration $\text{CDNC} = 200 \text{ cm}^{-3}$, ρ_w is the density of water, and σ is the width of a log-normal droplet distribution = 0.35. The MICROBASE retrievals provide an uncertainty estimate for each of its cloud microphysical retrievals based on a perturbation analysis performed for typical ranges of its input parameters (Zhao et al., 2014). The relative errors that MICROBASE products report in applying Eqs. (2) and (3) are estimated by perturbing their inputs (i.e., LWP). Zhao et al. (2014) reported this uncertainty in r_e at 5 %.

While these reported r_e errors suggest MICROBASE retrievals may be expected to have lower errors than our collocated SPHOT retrievals, these MICROBASE error estimates did not consider physical process uncertainty that stems from violations to above MICROBASE assumptions. For example, those standard products estimate r_e in Eq. (3) by assuming a default $\text{CDNC} = 200 \text{ cm}^{-3}$, a representative value for all-sky conditions at the SGP site. This value may be an appropriate assumption for midlatitude continental clouds, and its selection was informed through previous SGP radiative closure studies. This CDNC value may be significantly larger than expectations for marine Sc conditions $O(50 \text{ cm}^{-3})$ (e.g., Wood et al., 2015; Bennartz and Rausch, 2017; Wang et al., 2022). To test the validity of this default product assumption at ENA, we modified the standard retrieval to include an additional fixed $\text{CDNC} = 50 \text{ cm}^{-3}$ assumption. The authors also implemented a lower $\text{CDNC} = 100 \text{ cm}^{-3}$ test for SGP, as this CDNC is consistent with prior studies that contributed to MICROBASE development (e.g., Liao and Sassen, 1994). One physical argument for our need to consider a lower CDNC at SGP is that Sc cloud conditions that predominantly form within the hours following frontal passages may be associated with reduced aerosol.

Finally, there is ambiguity when defining an optimal strategy to compare our bulk, surface-based SPHOT retrievals to time-height MICROBASE r_e profiles. We consider the average 5 min in-cloud time-height r_e estimates from the

MICROBASE profiles. We also record the maximum MICROBASE value from within those clouds as a second reference. This is done for simplicity, as MICROBASE retrievals assume single-layer clouds, but allow for inhomogeneous cloud r_e profiles that yield different averaged behaviors in lower or upper parts of these clouds. As discussed later, one implication of these averages is that we should expect smearing of radar signatures or “critical” radius values associated with upper levels of the clouds and/or drizzle onset in time.

3 Results and Discussion: SGP Stratocumulus Clouds

This section summarizes results for SPHOT retrievals of cloud properties as collected from the Sc events over the SGP site. Data were drawn from 36 qualifying events that yielded 855 5 min comparisons between the various retrievals. For these Sc datasets, 26 events were associated with 645 additional comparisons from collocated TROPoe retrievals for LWP.

3.1 SGP Cloud Optical Depth, Effective Radius Retrievals and Liquid Water Path Estimates

In Fig. 2, we plot scatterplots (Fig. 2a) and box-whisker displays (Fig. 2b) for the SPHOT and MFRSR τ retrievals. Overall, τ comparisons between these instruments were associated with the highest coefficient of determination ($r^2 = 0.7$). As also reported in Chiu et al. (2012), retrievals from the SPHOT are larger than those from MFRSR measurements. For perfectly homogeneous clouds, retrievals from these two methods should be identical. However, clouds are never homogeneous and SPHOT τ will typically be larger than what is reported by MFRSR retrievals. This is because the transmitted flux measurement by the MFRSR monotonically decreases with increasing τ , following a convex curve (as shown in Fig. 3, for a $r_e = 8 \mu\text{m}$ at the 440 nm channel). For inhomogeneous clouds and assuming no wind, the MFRSR measures an averaged flux that will always correspond to an equal or smaller τ than the average obtained from the τ values inferred from a SPHOT. The magnitude of this systematic difference between MFRSR- and SPHOT-based retrieval depends on the degree of cloud inhomogeneity.

For this study, we report Bias = $\langle \Delta \rangle$ and the Root Mean Square Error $\text{RMSE} = (\langle \Delta^2 \rangle)^{1/2}$. The Δ is the difference between the SPHOT retrieval and the similar quantity from the reference instrument. Overall, τ retrieval distributions indicate a higher SPHOT median (24.5) to the MFRSR (18.1), and extended quartiles/tail. The $\text{RMSE} = 2.79$ (unitless, relative error > 10 %) between these units is larger than retrieval uncertainty typically reported for either instrument with respect to algorithm perturbation tests (τ error < 2, relative error < 5 %).

SGP retrieval intercomparisons for r_e are summarized in Fig. 4. In Fig. 4a, we plot relative performance when com-

pared to the default MICROBASE implementation, while Fig. 4b plots the MICROBASE retrieval behavior if applying a modified assumption for fixed $\text{CDNC} = 100 \text{ cm}^{-3}$. In Fig. 4c, we plot a reference maximum r_e from the default MICROBASE during each 5 min sample. Summary box and whisker displays for all r_e estimates are plotted in Fig. 4d.

Overall, relative SPHOT-MICROBASE comparisons highlight a shift towards lower bias when MICROBASE retrievals at SGP adopt the lower fixed CDNC. However, most pairings exhibit negligible retrieval correlations, with this low-bias $\text{CDNC} = 100 \text{ cm}^{-3}$ configuration reporting an $r^2 < 0.1$ and a RMSE of $2.38 \mu\text{m}$. SPHOT retrieved r_e median value(s) and quartile distributions skew larger than ranges estimated by the other instruments (median $r_e = 10.81 \mu\text{m}$), with the largest discrepancies found between SPHOT and MICROBASE’s default $\text{CDNC} = 200 \text{ cm}^{-3}$ (median $r_e = 5.01 \mu\text{m}$). Some offset between MICROBASE and SPHOT should be expected, since both retrievals cannot properly attribute and distribute profile water content in the presence of drizzle. In the case of MICROBASE’s r_e estimates in Eq. (3), the LWC assumes a cloud droplet distribution (i.e., a larger number of only slightly larger drops) rather than attributing some liquid to a few larger drizzle droplets at the expense of small particles. Similarly, SPHOT r_e will be skewed high in the presence of drizzle, as absorption at the 1640 nm channel will increasingly act towards solutions having larger r_e . Previous studies suggest a “critical” effective radius for drizzle onset as associated with a cloud top r_e of “at least 12” to $14 \mu\text{m}$ (e.g., Rosenfeld and Gutman, 1994; Lebsock et al., 2011; Rosenfeld et al., 2012). Considering those previous statements are associated with observations or modeling performed near cloud top and/or at finer resolution, we use such values only as a guideline that the median SPHOT properties we retrieve of $11 \mu\text{m}$ suggests the common presence of drizzle within our SGP samples. As introduced above, our temporal averaging combined with the FOV of the observations may result in our sampling of lower r_e retrieval values that are consistent with drizzle in the cloud above. Moreover, since surface-based photometer measurements are less constrained to the upper-levels of Sc when drizzle is forming (i.e., the observed radiance at the surface is dictated by the entire cloud layer), previous cloud top statements specific to cloud top may be better suited to intrinsic drizzle onset in r_e , whereas photometer measurements should experience lag or partial influences as that drizzle falls through the cloud.

In Fig. 5a, we plot a scatterplot for the LWP estimated by SPHOT following Eq. (1) versus estimates from the MWR. In Fig. 5b and c, the cumulative distributions for these comparisons are provided, as well as LWP comparisons when TROPoe products were available. There is solid agreement between the SPHOT and “Version 1” of the MWRRET LWP estimates, with $r^2 = 0.46$ and RMSE of 6.38 g m^{-2} . At SGP, ARM offers two versions of MWR estimates, with a “Version 2” utilizing the MWR’s 89 GHz frequency to better sep-

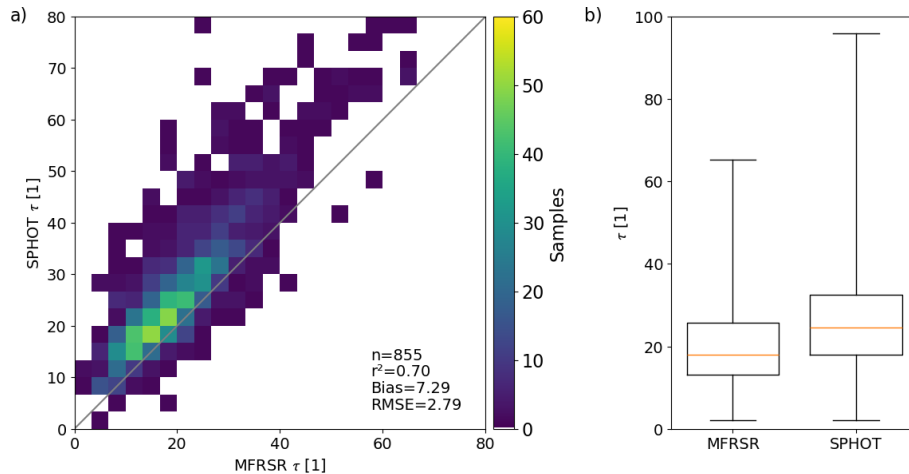


Figure 2. (a) Scatterplot of cloud optical depth τ retrievals (unitless, bin size 3.2) from the SPHOT and MFRSR. (b) Associated SPHOT and MFRSR box and whisker plots for τ distribution quartiles and extremes, with distribution medians in yellow.

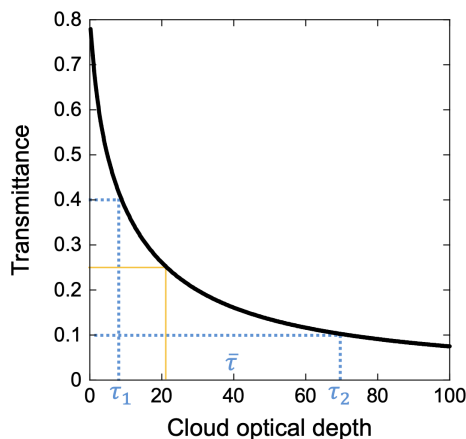


Figure 3. Example relationship between the transmittance and cloud optical depth (τ), as denoted by the solid black curve ($r_e = 8 \mu\text{m}$ at the 440 nm channel). Suppose an inhomogeneous scene containing two optical depths (e.g., τ_1 and τ_2 that lead to transmittances of 0.4 and 0.1, respectively), shown by dotted blue lines. Due to its hemispherical FOV, the MFRSR would measure an averaged transmittance (i.e., 0.25) and a retrieved τ of ~ 20 (orange lines). In contrast, SPHOT with a narrow FOV would retrieve τ_1 and τ_2 , leading to an average $\bar{\tau}$ of ~ 40 .

arate the contributions of drizzle to the LWP. Note that the MWRRET “Version 2” products and TROPoe LWP estimate comparisons indicate a lower median and narrower spread of LWP estimates (we find a median value of 70.2 g m^{-2} from TROPoe compared to 136.9 g m^{-2} from SPHOT). An explanation for these discrepancies is the presence of drizzle, potentially responsible for the key differences that occur at higher-relative r_e levels. A high-relative SPHOT LWP bias is common at SGP, and found to lower-relative r_e values than for ENA Sc events (Sect. 4). We suggest this may be tied to the higher CDNC conditions and wider retrieval spread in

the less quiescent post-frontal SGP Sc conditions, allowing higher τ and/or LWP that are consistent with drizzle presence at lower r_e .

3.2 Discussion of Cumulative SGP Sc Retrieval Performance

While SPHOT retrievals at SGP are found in modest agreement with the collocated sensors – with an emphasis on non-drizzling Sc conditions – it is important to consider potential controls on retrieval variability. In Fig. 6, scatterplots from the previous section have been sorted according to a second retrieved quantity. In Fig. 6a and b, we plot τ performance indexed according to their associated LWP and r_e retrievals, respectively. As before, SPHOT overestimates the values obtained from the MFRSR, with larger τ associated with larger LWP as expected. Most discrepancies we observe are physically consistent, i.e., higher offsets in τ are associated with samples where SPHOT retrieved smaller r_e (i.e., r_e values $< 7\text{--}8 \mu\text{m}$). Large offsets were observed for cases with moderate LWP $O[150\text{--}200 \text{ g m}^{-2}]$ (Fig. 5a).

In Fig. 6c and d, we plot r_e retrievals indexed according to τ and LWP. The largest discrepancies between SPHOT and the MICROBASE techniques for r_e estimates are found at lower values of τ and within an intermediate range of LWP values where the SPHOT r_e can be significantly larger. For larger optical thicknesses and LWP, the effective radius estimated by MICROBASE can be much larger than that from SPHOT. This behavior aligns with retrieval susceptibility to larger errors near conditions of drizzle onset. Overall, the SPHOT retrievals are higher than our adjusted MICROBASE estimates for r_e , consistent with previous findings (i.e., Fig. 4d). This follows as the MICROBASE approach is unable to partition LWP to r_e appropriately under drizzling conditions. Breakdowns for the estimated LWP from the SPHOT (Fig. 6e and f) indicate that increasing

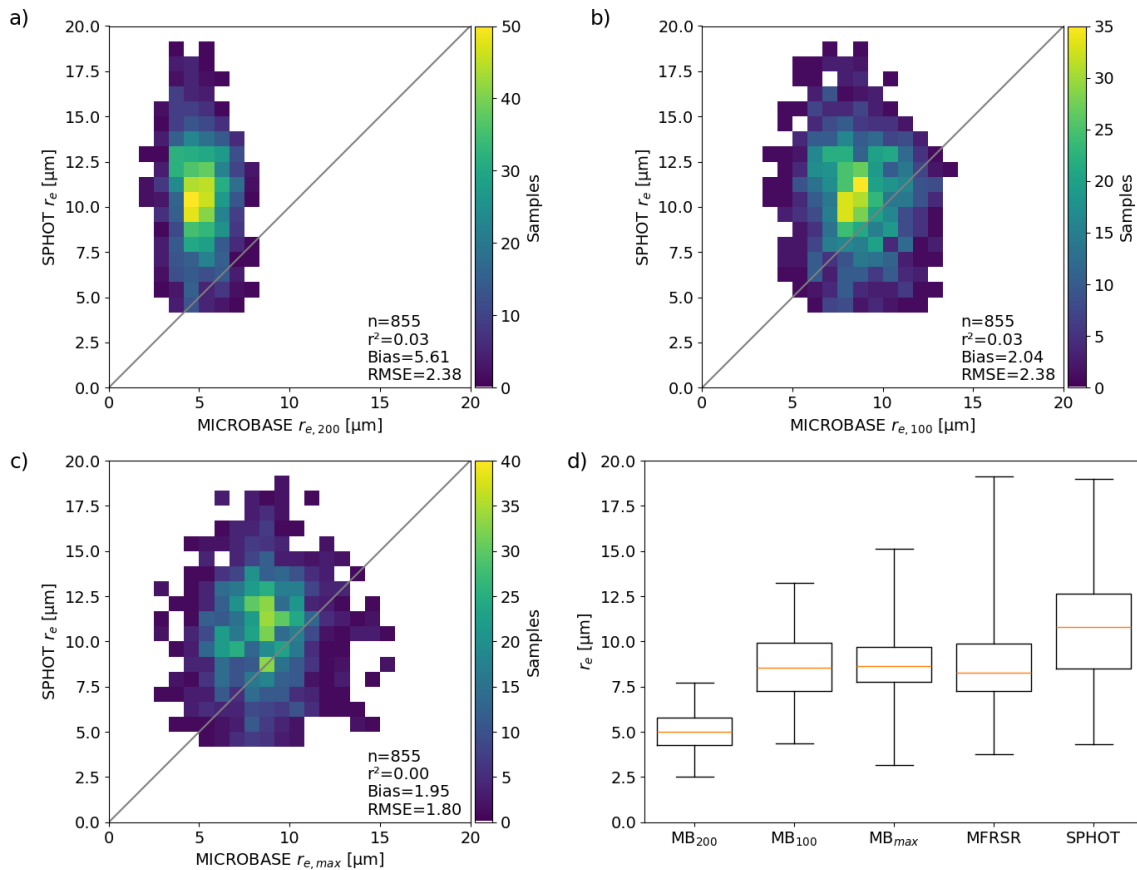


Figure 4. Scatterplots of r_e retrievals with associated R^2 , Bias and RMSE [μm , bin size $0.8\ \mu\text{m}$] from the SPHOT and MICROBASE with (a) MICROBASE CDNC assumption of $200\ \text{cm}^{-3}$, (b) MICROBASE CDNC assumption of $100\ \text{cm}^{-3}$, (c) selection of the maximum MICROBASE r_e in the column (using CDNC = $200\ \text{cm}^{-3}$). (d) SPHOT, MICROBASE, and MFRSR box and whisker plots for r_e distribution quartiles and extremes, with distribution medians in yellow.

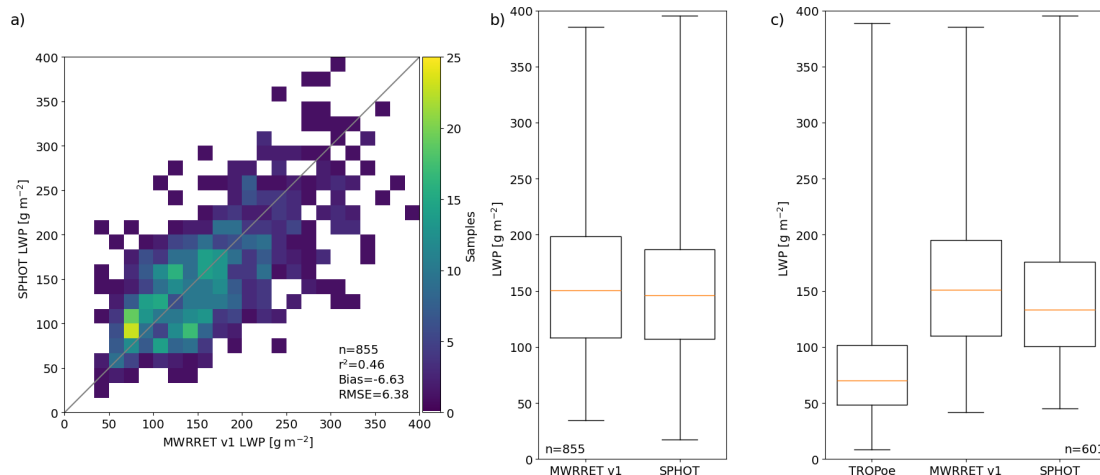


Figure 5. (a) Scatterplot of LWP retrievals and associated R^2 , Bias and RMSE [g m^{-2} , bin size $16\ \text{g m}^{-2}$] from the SPHOT and MWRRET (“Version 1”). Box and whisker plots for LWP distribution quartiles and extremes, with distribution medians in yellow for (b) cumulative SPHOT and MWRRET datasets, and (c) datasets including TROPoe product availability.

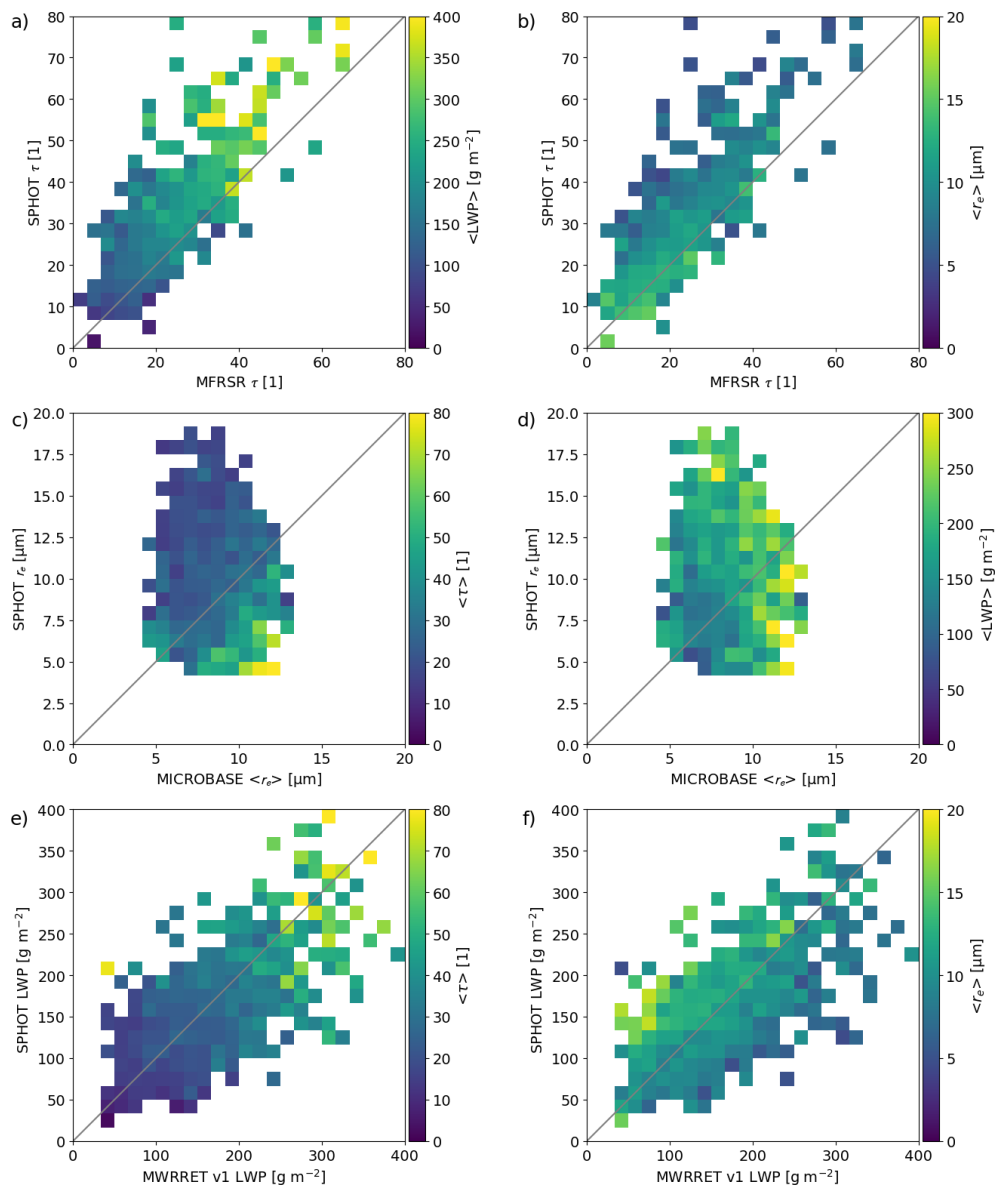


Figure 6. For SGP events, (a, b) scatterplots of SPHOT and MFRSR τ retrievals contingent on r_e and LWP retrievals from the SPHOT. (c, d) SGP scatterplots of SPHOT and MICROBASE r_e retrievals contingent on τ and LWP retrievals from the SPHOT. (e, f) SGP scatterplots of SPHOT and MWRRET “Version 1” LWP retrievals contingent on τ and r_e retrievals from the SPHOT. Bin sizes: 2.4, 0.8 μm , and 16 g m^{-2} .

LWP scales with increasing τ , while LWP offsets are relatively unbiased or insensitive to the bulk magnitude of τ estimates. However, lower magnitude r_e values from the SPHOT are those that occupy the relatively lower-biased LWP estimate space, and larger r_e values are associated with relative SPHOT overestimates of LWP. This response is physically consistent with Eq. (1), with larger r_e shifts (i.e., presence of drizzle) compensated by smaller, yet important shifts in τ estimates (high bias, yet commensurate with drizzle). This argument may also be consistent with SPHOT and MWRRET “Version 1” versus “Version 2” performances relative to the

TROPoe approach with respect to the role small amounts of drizzle drive on LWP disconnects between these instruments.

In Fig. 7, we plot the relative error for LWP estimates between SPHOT and TROPoe products as a function of the r_e estimated by the SPHOT. SPHOT LWP discrepancies compared to TROPoe estimates are increasing to higher r_e , with these differences potentially exacerbated once $r_e > 10 \mu\text{m}$. These fractional differences may reflect complications associated with drizzle, including the possible use of samples from times adjacent to surface precipitation (e.g., water remaining on the instruments). Moreover, drizzle onset/presence is suggested as one factor in these discrepancies when

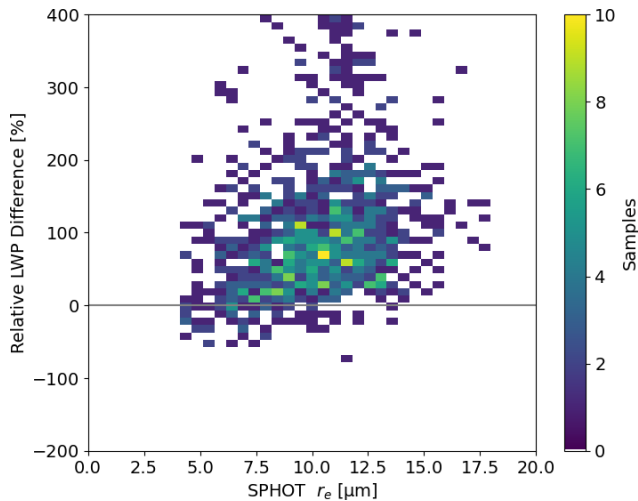


Figure 7. Scatterplot for the relative difference (SPHOT minus TROPoe retrieval divided by the TROPoe retrieval) in LWP estimates as a function of the associated SPHOT r_e retrieval estimate (bin size $0.5 \mu\text{m}$ and 10g m^{-2}).

these results are compared with ENA findings to follow, but not the sole explanation for the LWP estimate offsets. Select overestimation of the LWP by the SPHOT method may also be attributed to spatial inhomogeneity captured differently by the narrower FOV instrument or methods that combine observations having different FOVs (factors that may also promote higher SPHOT τ when compared to the MFRSR).

In Table 1, we list SPHOT breakdowns for SGP clouds contingent on ARSCL-estimated cloud thickness. Thicker clouds show increasing values for τ and LWP. An absence of a similar trend in r_e behaviors may be tied to SGP variability in CDNC and drizzle propensity under higher LWP often consistent with drizzle for marine locations (e.g., Rosenfeld et al., 2012; Zhu et al., 2022). The standard deviations for retrievals vary according to the thickness and drizzle likelihood, with thicker clouds associated with a larger retrieval spread. Standard deviations for τ are larger than the values from algorithm perturbation tests, yet of similar magnitude to the RMSE observed between collocated MFRSR and SPHOT estimates. r_e estimates sorted according to cloud thickness bins share relative standard deviation variability comparable to the uncertainty claims from retrieval perturbation and RMSE discrepancies as before. Overall, averaging within the cloud thickness bins reduces the event-scale physical process variability, with standard deviations consistent with retrieval uncertainty suggested prior.

Each cloud thickness bin for SGP exhibits bulk LWPs exceeding 100g m^{-2} , with τ values typically exceeding 20. For marine clouds, such values would be consistent with copious drizzle (e.g., Zhu et al., 2022). We report radar mean Doppler velocity averages in SGP Sc clouds (the last columns of Table 1) to potentially identify shifts in mean downward air motions suggestive of drizzle. However, all values we observe at

SGP as a function of cloud thickness are downwards, and far exceed average motions found for similar clouds/thickness at ENA. This is likely because SGP observations are collected during post-frontal conditions, with vertical wind shear and larger-scale flows that contaminate radar velocity estimates more than would be expected for quiescent ENA Sc. These factors render simple uses of mean Doppler velocity at SGP far less informative to drizzle onset than forthcoming ENA examples.

4 Results and Discussion: ENA Stratocumulus Clouds

This section presents summary results as collected during qualifying marine Sc events at the ENA site. These data were drawn from 80 qualifying events that provided 1341 5 min comparisons between the various instruments. For these datasets, 41 events with 627 samples were available from collocated TROPoe LWP estimates.

4.1 ENA Retrieval Performance

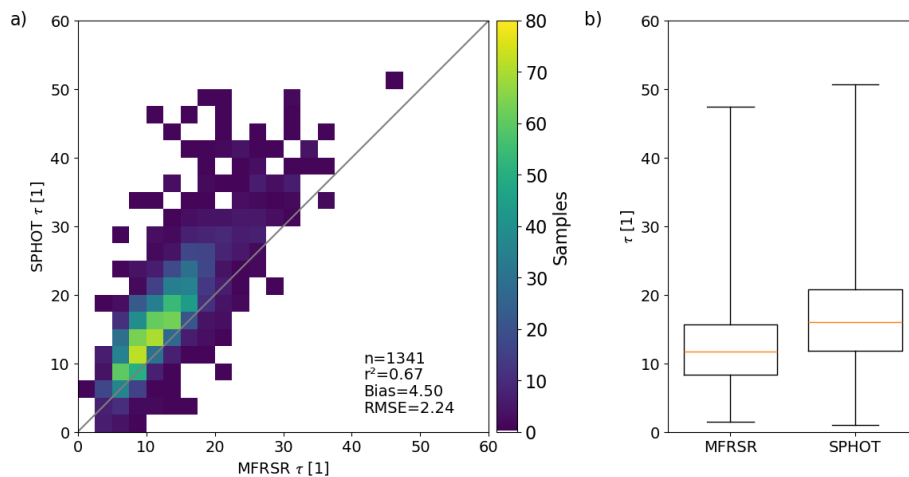
In Figs. 8–10, we repeat SGP comparison plots for ENA. One notable change is the inclusion of a MICROBASE $\text{CDNC} = 50 \text{cm}^{-3}$ to accompany the baseline $\text{CDNC} = 200 \text{cm}^{-3}$ retrieval. Similar trends with SGP are observed, including a high offset for τ from the SPHOT compared to the MFRSR (Fig. 8a and b). For the ENA site, only “Version 2” of the MWRRET products were available. The Sc τ at ENA are lower, reflected by a dataset median value = 16.0 that is 2/3rds of the value from our SGP dataset. Adjusting the default MICROBASE assumption to $\text{CDNC} = 50 \text{cm}^{-3}$ provides agreement with collocated r_e retrievals (Fig. 9a and b). We find a relatively similar median r_e near $10 \mu\text{m}$ that is comparable to values estimated for SGP. In terms of LWP comparisons (Fig. 10a–c), the lower τ clouds associated with a similar r_e implies ENA as having lower LWP values than typical SGP Sc. Overall, LWP estimates suggest lower standard errors than those from SGP Sc events (Fig. 10b). We attribute improved comparisons to ENA’s lesser propensity for drizzle, where SPHOT and TROPoe retrievals are reporting LWP at similar levels for most r_e values retrieved (Fig. 11). This improvement may also be coupled to the lower attendant CDNC conditions and reduced variability in CDNC also improving relative comparisons. We still observe SPHOT methods tend to overestimate LWP surrounding likely conditions with drizzle onset where bulk $r_e > 12.5 \mu\text{m}$ (Fig. 11).

4.2 Discussion of Cumulative ENA Retrieval Performance

In Fig. 12, we plot ENA comparisons contingent on select jointly retrieved quantities. For these examples, we have included references to the KAZR in-cloud mean Doppler velocity averages during the 5 min sampling window. For

Table 1. A summary of SGP Sc cloud properties and SPHOT retrievals contingent on cloud thickness. The MDV refers to the average in-cloud mean Doppler velocity from KAZR over the sampling window.

Cloud Thickness [m]	# obs	$\langle \tau \rangle$ [1]	SD(τ) [1]	r_e [μm]	SD(r_e) [μm]	LWP [g m^{-2}]	SD(LWP) [g m^{-2}]	MDV [ms^{-1}]	SD(MDV) [ms^{-1}]
200–400	86	18.92	8.42	11.01	3.53	107.99	39.58	−0.11	0.38
400–600	224	24.9	9.59	10.52	2.59	139.51	49.7	−0.18	0.35
600–800	180	27.72	14.27	10.48	2.61	150.25	57.77	−0.22	0.34
800–1000	118	30.89	16.41	10.84	2.8	169.66	64.24	−0.19	0.36
1000–1200	89	32.6	16.41	10.12	3.35	168.64	73.88	−0.28	0.35
> 1200	157	29.88	11.86	10.98	3.23	171.81	57.18	−0.2	0.32

**Figure 8.** As in Fig. 2, but for ENA Sc τ samples from the SPHOT and MFRSR.

ENA, these estimates may serve as a better proxy for the presence of drizzle than what was found for post-frontal SGP Sc conditions. Summary retrieval performances as a function of cloud thickness for cumulative ENA clouds are found in Table 2. For these tables, we have included extra columns that report the number/percentage of ENA samples where ARSCL recorded reflectivity factor Z exceeding a -20 dBZ threshold below the ARSCL (ceilometer) estimated cloud base (we assume this is accurate to within a few radar gates of 90 m below, e.g., Zhu et al., 2024). These below cloud signatures may act as a proxy for clouds with more substantial drizzle at ENA (e.g., Yang et al., 2018). Such signatures were not viable at SGP because insect contamination below the cloud limits using these echoes without applying decluttering techniques (e.g., Williams et al., 2021).

As observed with SGP events, higher τ estimates are associated with higher mean LWPs. The mean Doppler velocity signatures help demonstrate a pronounced shift within ENA clouds once sufficient drizzle is present (for cloud LWPs exceeding 100 g m^{-2} and associated τ that exceeds 20). Larger r_e values are also often associated with larger LWP, with clouds exceeding LWP of 200 g m^{-2} typically exhibiting $r_e > 12 \mu\text{m}$ from SPHOT and downward mean Doppler velocity consistent with drizzle (Fig. 12b and d). These prop-

erties are qualitatively consistent with SGP, where LWP estimates are higher under conditions where the SPHOT r_e estimates are larger (Fig. 12e). Overall, Doppler velocity characteristics suggest downward motions and drizzle within these ENA Sc clouds once LWP exceeds 100 g m^{-2} and/or bulk r_e from the photometer exceeds $12 \mu\text{m}$ (Fig. 12f).

In Table 2, cumulative ENA SPHOT performances as a function of cloud thickness follow expectations from previous marine Sc studies (e.g., Zhu et al., 2022). ENA clouds having a similar cloud thickness to SGP clouds indicate similar mean r_e values, however ENA clouds indicate a reduced τ compared to SGP, and therefore reduced LWP following calculations in Eq. (1). For example, a typical 500 m ENA cloud thickness records a LWP of 80 g m^{-2} with an τ of 15; the similar SGP Sc cloud is associated with large shifts in τ (25) and LWP (140 g m^{-2}). Physically, this follows from an expectation that SGP Sc are associated with double the CDNC value, though other differences between post-frontal and marine Sc may also contribute (e.g., Mechem et al., 2010). For marine clouds, we commonly observe Z echoes exceeding our -20 dBZ threshold below the cloud base and a prominent shift in the mean Doppler velocity once relative LWPs exceed 100 g m^{-2} or cloud thickness exceeds 1 km. Approximately 80 %–90 % of the Sc clouds with thickness greater

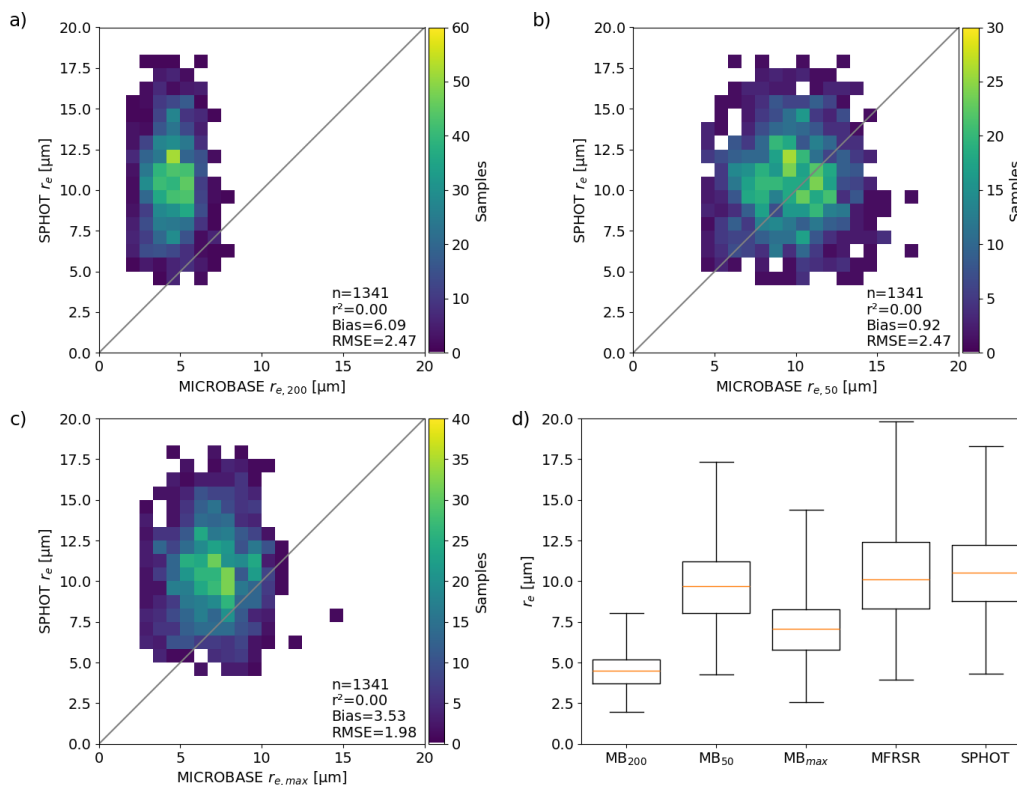


Figure 9. As in Fig. 4, but for ENA r_e samples from the SPHOT, MICROBASE, and MFRSR. For the ENA dataset, a MICROBASE CDNC = 50 cm^{-3} assumption has been substituted for the previous SGP assumption of CDNC = 100 cm^{-3} .

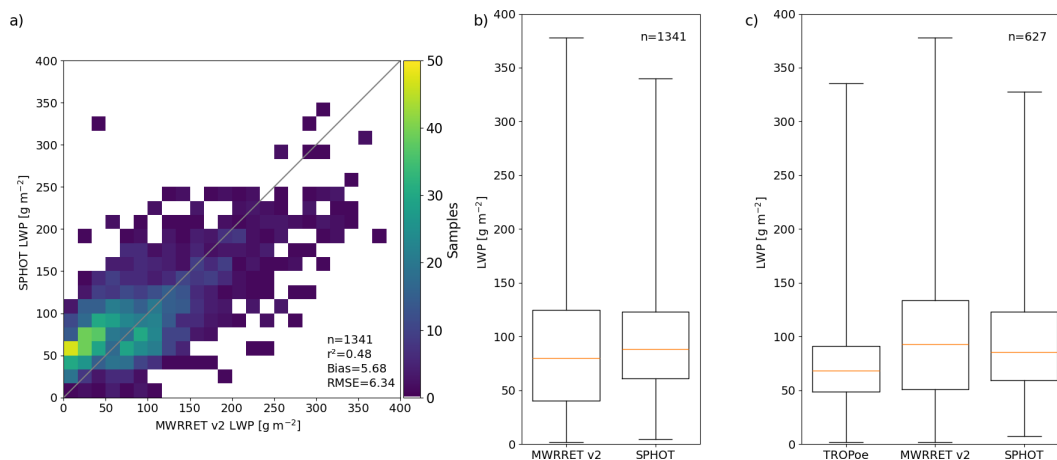


Figure 10. As in Fig. 5, but for ENA LWP estimates. For the ENA dataset, MWRRET “Version 2” retrievals have been substituted as “Version 1” is unavailable at the site.

than 1.0 km indicate drizzle below the cloud base (bulk cloud $r_e > 12\ \mu\text{m}$). All thickness bins at ENA report some percentage of samples having this form of proxy subcloud drizzle signatures.

4.3 Potential Island Influences on ENA Sc Properties?

Several recent studies discuss the potential role that islands, such as ENA’s Graciosa Island and its terrain or waves emanating off the surrounding islands in the Azores archipelago, may have on influencing the clouds and precipitation over those islands (Houze, 2012). These studies often do not place as much emphasis on the expectations for Sc and anticipated

Table 2. As in Table 1, a summary of ENA Sc cloud properties and SPHOT retrievals contingent on cloud thickness. BC columns refer to the number and % of samples having measurable (> -20 dBZ) KAZR reflectivity factor at 90 m below the estimated cloud base from the ARM ARSCL VAP.

Cloud Thickness [m]	# obs	$\langle \tau \rangle$ [1]	SD(τ) [1]	r_e [μm]	SD(r_e) [μm]	LWP [g m^{-2}]	SD(LWP) [g m^{-2}]	MDV [m s^{-1}]	SD(MDV) [m s^{-1}]	BC	BC %
200–400	220	11.43	4.64	10	2.29	59.36	23.76	−0.01	0.06	2	0.91
400–600	395	14.88	5.83	10.05	2.24	80.04	34.55	−0.01	0.07	79	20
600–800	342	17.96	7.4	10.52	2.57	101.02	41.76	−0.01	0.08	200	58.48
800–1000	201	21.23	8.36	10.96	2.65	125.83	50.47	−0.03	0.09	171	85.07
1000–1200	74	20.69	7.25	11.97	3.01	132.58	47.64	−0.04	0.16	69	93.24
> 1200	103	26.59	9.44	12.04	3.43	171.47	64.45	−0.18	0.29	92	89.32

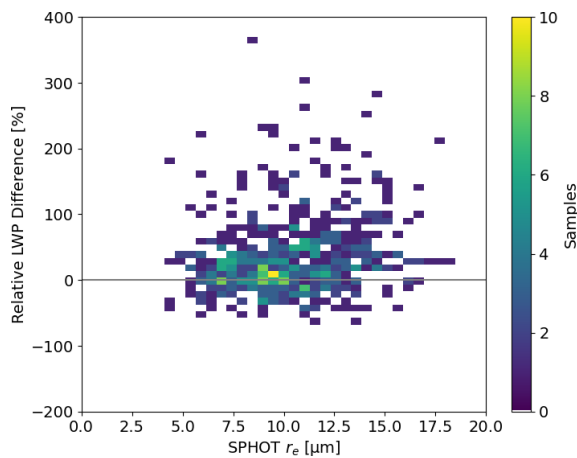


Figure 11. As in Fig. 7, but for ENA site.

impacts on the likelihood of precipitation that may lessen the usefulness of profiling retrievals (such as ARM-style measurements collected on islands) as representative of wider open ocean Sc cloud properties. For an ENA site located on the northern coastline of the island, studies by Giangrande et al. (2019) have suggested the influence that larger-scale southerly flow may play on overall cloud thickness or drizzle/rain properties observed over an upwind site. Ghate et al. (2021) and Jeong et al. (2022) also indicated shifts in sub-cloud turbulence and in-cloud air motions using Doppler lidar or cloud radar observations on days when surface winds come from directions associated with island versus onshore ocean flows. Moreover, it is common that recent ENA studies remove all such “island” flow complexities from their analyses, avoiding many conditions that promote shallow and Sc clouds over the site (e.g., Mechem et al., 2018). While such complex interactions over the Azores archipelago deserve a dedicated study beyond the scope of the current study, the authors were interested in whether extended photometer Sc retrievals suggest similar and/or significant shifts in cloud properties contingent on these flows over Graciosa.

In Tables 3 and 4, we include an ENA breakdown for “island” versus “ocean” wind events, applying similar definitions to those found in Ghate et al. (2021). For this site,

“ocean” winds are those from 315 to 90°. For cloud retrievals from this ENA dataset, the “island” cloud days exhibit slightly larger values of LWP and τ for relatively similar r_e ; however, the differences we observe in mean τ /LWP characteristics are within the standard errors for clouds of that given thickness, and within measurement uncertainty for most individual retrievals. There is a suggestion that clouds upwind under island flows may have a higher propensity for drizzle formation (if based on using LWP increase as a proxy). However, several corroborating signatures – such as the enhancements in mean Doppler velocity – may also be attributed to more frequent gravity waves at cloud level commonly observed around the islands with flow over terrain. Similarly, flow over the islands may be associated with higher aerosol and/or CDNC, offsetting higher LWP in terms of potential for drizzle onset.

Although our sampling that is contingent on cloud thickness is independent and non-sequential, using significance tests such the Student’s t test on any differences we observe is typically not appropriate for these applications given the skewness of the cloud property distributions we are sampling. Mann–Whitney significance tests (e.g., Mann and Whitney, 1947) suggest that differences we observe in r_e , mean Doppler velocity, and/or LWP may be significant, but with the caution that these tests also provide occasional contradictory results (i.e., for select results in thickness bins). Overall, our current dataset suggests that the role of these islands on the retrieved Sc cloud properties (however, requiring widespread Sc clouds that are already present at daytime) is inconclusive, potentially suggesting only minor enhancements in longer-track cloud averages that may be otherwise indistinguishable on an individual event/sample basis. The authors suggest that “island” sensitivity may be more pronounced if considering a wider range of synoptic-scale forcing, cloud types, or observations (e.g., dynamical versus microphysical properties), as was found in efforts such as Giangrande et al. (2019) or Jeong et al. (2022).

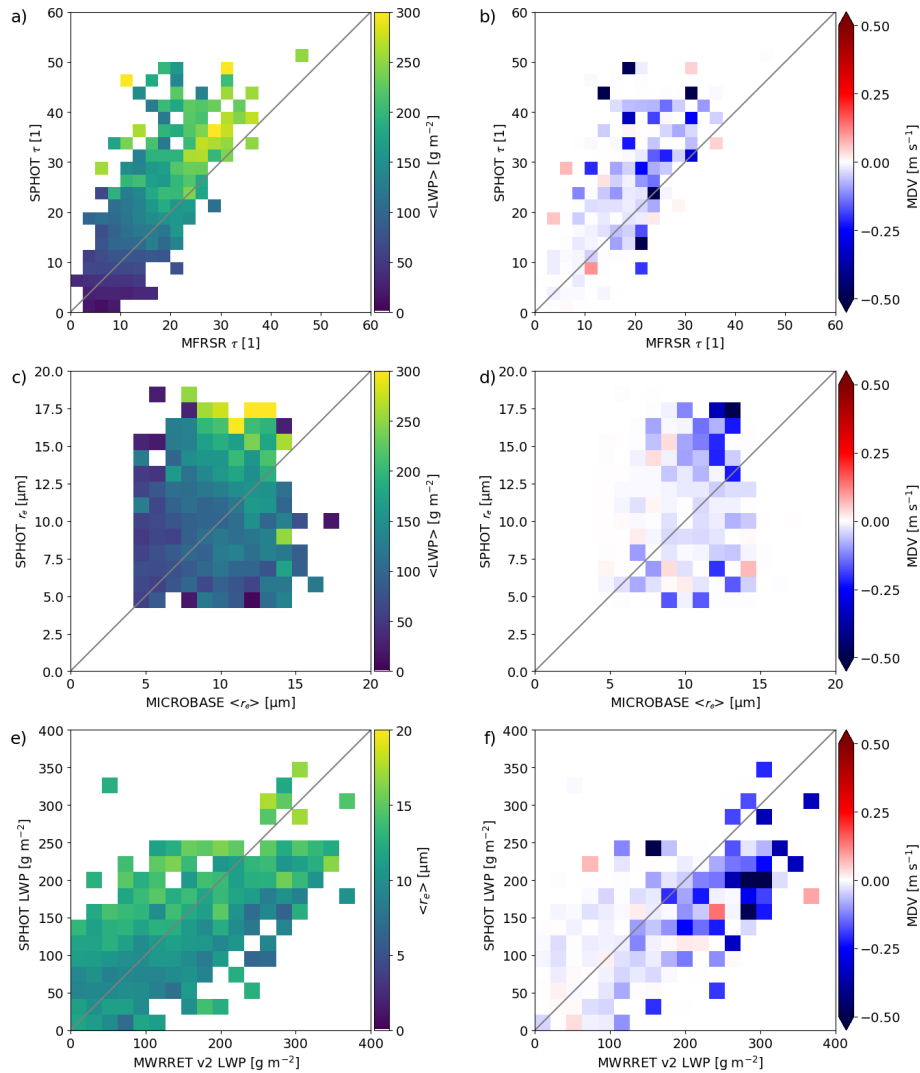


Figure 12. For ENA events, (a, b) scatterplots of SPHOT and MFRSR τ retrievals contingent on LWP from the SPHOT and mean Doppler velocity estimates from KAZR. (c, d) ENA scatterplots of SPHOT and MICROBASE r_e retrievals contingent on LWP from the SPHOT and mean Doppler velocity estimates from KAZR. (e, f) ENA scatterplots of SPHOT and MWRRET “Version 2” LWP retrievals contingent on r_e from the SPHOT and mean Doppler velocity estimates from KAZR. Bin sizes: 2.4, 1 μm , and 20 g m^{-2} .

Table 3. As in Table 2, a summary of ENA Sc cloud properties and SPHOT retrievals contingent on cloud thickness with surface winds from southerly island-influenced directions (from 90° E to 315° WNW).

Cloud Thickness [m]	# obs	$\langle \tau \rangle$ [1]	SD(τ) [1]	r_e [μm]	SD(r_e) [μm]	LWP [g m^{-2}]	SD(LWP) [g m^{-2}]	MDV [m s^{-1}]	SD(MDV) [m s^{-1}]	BC	BC %
200–400	117	12.54	4.5	9.57	2.16	62.95	23.11	−0.02	0.08	0	0
400–600	173	15.64	6.21	10.58	2.24	88.53	35.53	−0.02	0.09	29	16.76
600–800	141	18.32	8.33	10.52	2.42	102.68	44.19	−0.02	0.12	83	58.87
800–1000	58	20.91	7.74	10.95	2.39	124.01	44.09	−0.02	0.08	48	82.76
1000–1200	22	21.26	5.55	11.94	3.13	137.41	42.03	−0.06	0.27	18	81.82
> 1200	21	26.04	9.73	11.61	3.43	160.83	55.96	−0.15	0.26	17	80.95

Table 4. As in Table 3, a summary of ENA Sc cloud properties and SPHOT retrievals contingent on cloud thickness. Surface winds for these samples are those from northerly oceanic-influenced directions (from 315° WNW to 90° E).

Cloud Thickness [m]	# obs	$\langle\tau\rangle$ [1]	SD(τ) [1]	r_e [μm]	SD(r_e) [μm]	LWP [g m^{-2}]	SD(LWP) [g m^{-2}]	MDV [m s^{-1}]	SD(MDV) [m s^{-1}]	BC	BC %
200–400	103	10.17	4.47	10.49	2.34	55.29	23.83	0	0.02	2	1.94
400–600	222	14.29	5.45	9.64	2.15	73.42	32.26	−0.01	0.06	50	22.52
600–800	201	17.7	6.65	10.52	2.67	99.86	39.93	0	0.04	117	58.21
800–1000	143	21.37	8.6	10.97	2.75	126.57	52.82	−0.03	0.1	123	86.01
1000–1200	52	20.45	7.84	11.99	2.97	130.54	49.68	−0.04	0.07	51	98.08
> 1200	82	26.73	9.36	12.16	3.43	174.2	66.17	−0.19	0.3	75	91.46

5 Conclusions

This study presents cloud properties and instrument comparisons performed following the automating of a set of retrievals from photometers. This effort documents longer-term breakdowns of key relative retrieval performances for τ , r_e and LWP within marine and continental Sc clouds. Overall, the performance at the fixed ENA and SGP sites provides confidence and initial uncertainty references for 3-channel retrieval methods to be similarly automated for non-vegetated surfaces and remote locations where 2-channel retrievals were not previously viable. Key takeaways from this study are summarized as follows:

- Photometer τ retrievals are offset high when compared to retrievals obtained from the wider FOV MFRSR. Photometer r_e retrievals are offset high relative to MFRSR and MICROBASE estimates, primarily under conditions when drizzle is likely present. The LWP calculated from SPHOT τ and r_e is relatively unbiased when compared to collocated LWP references under settings without drizzle and/or within lower or less complex CDNC contexts.
- Stratocumulus conditions at SGP and ENA exhibit substantially different τ and LWP magnitudes for similar bulk r_e estimates, as attributable to differences in CDNC levels between these regions. The typical SGP Sc exhibits double the τ and LWP as the one observed at ENA; For similar cloud thickness, the Sc clouds at ENA and SGP share comparable r_e that highlight propensity for Sc at both locations to form drizzle.
- Potential “drizzle” signatures become increasingly apparent once bulk SPHOT cloud r_e estimates exceed 12 μm . ARM’s baseline MICROBASE retrievals were modified from their standard assumptions (CDNC = 200 cm^{-3}) to align with photometer r_e retrievals. These changes suggest CDNC values near 50 and 100 cm^{-3} for cleaner ENA and “post-frontal” SGP conditions, respectively.
- Simple tests for “island” versus “ocean” wind conditions as a proxy for local ENA island controls on

Sc properties were performed. While cloud conditions having flows over the “island” potentially promoted higher τ , LWP or drizzle propensity for clouds of similar thickness (to significance testing standards), these enhancements were small and within typical instrument sampling/retrieval errors.

Code and data availability. All ARM data including the “AR-SCL”, “MET”, “SPHOTCOD2CHIU”, “MFRSRCLDOD”, and “MICROBASEKaPlus” named “value-added product” or “VAP” datasets used by this study can be downloaded at <https://www.arm.gov/> (last access: 2 February 2025). These data and VAP code requests may be access through the ARM Data Center “Data Discovery” portal found at: <https://adc.arm.gov/discovery/#!/> (last access: 15 August 2025).

Author contributions. JR, LM, DW, SG, CSH, and MW contributed to preparing ARM data products and troubleshooting therein. KS, SG, and JR planned the experiments and comparisons. LM, CC, and CSH collected, processed and helped troubleshoot sunphotometer instrument data and automatic retrievals therein. All authors contributed to the scientific discussion and to the writing of this paper.

Competing interests. The contact author has declared that none of the authors has any competing interests.

Disclaimer. Publisher’s note: Copernicus Publications remains neutral with regard to jurisdictional claims made in the text, published maps, institutional affiliations, or any other geographical representation in this paper. While Copernicus Publications makes every effort to include appropriate place names, the final responsibility lies with the authors. Views expressed in the text are those of the authors and do not necessarily reflect the views of the publisher.

Acknowledgements. This paper has been authored by employees of Brookhaven Science Associates, LLC, under contract DE-SC0012704 with the U.S. DOE. The publisher by accepting the paper for publication acknowledges that the United States Government retains a nonexclusive, paid-up, irrevocable, worldwide license to publish or reproduce the published form of this paper, or

allow others to do so, for United States Government purposes. We acknowledge support from the Atmospheric Radiation Measurement (ARM) program, a user facility of the U.S. DOE, Office of Science, sponsored by the Office of Biological and Environmental Research. Additional support was from the Atmospheric Systems Research (ASR) program of that office. All ARM data sets used for this study can be downloaded at <http://www.arm.gov> (last access: 15 August 2025) and associated with several VAPs as previously noted in the “Data availability” section. We also would like to thank the ARM’s Data Center (<https://www.arm.gov/data/>, last access: 15 August 2025) for their support, account access, and interactions therein. The authors would like to acknowledge the extended team efforts of ARM developers at Brookhaven National Laboratory working with science sponsors and mentors, including initial code conversions and design reviews performed by Tami (Toto) Fairless. Additional thanks from the authors is extended to Karen Johnson (BNL), Damao Zhang (PNNL), David Mechem (KU) and Dave Turner (NOAA, GSL) for helpful discussions on this manuscript.

Financial support. This research has been supported by the US Department of Energy (grant nos. DE-SC0012704 and DE-SC0021167). This project was supported in part by the U.S. Department of Energy, Office of Science, Office of Workforce Development for Teachers and Scientists (WDTS) under the Science Undergraduate Laboratory Internships Program (SULI).

Review statement. This paper was edited by Piet Stammes and reviewed by Israel Silber and one anonymous referee.

References

- Albrecht, B. A.: Aerosols, cloud microphysics, and fractional cloudiness, *Science*, 245, 1227–1230, 1989.
- Bennartz, R. and Rausch, J.: Global and regional estimates of warm cloud droplet number concentration based on 13 years of AQUA-MODIS observations, *Atmos. Chem. Phys.*, 17, 9815–9836, <https://doi.org/10.5194/acp-17-9815-2017>, 2017.
- Bony, S. and Dufresne, J.-L.: Marine boundary layer clouds at the heart of tropical cloud feedback uncertainties in climate models, *Geophys. Res. Lett.*, 32, L20806, <https://doi.org/10.1029/2005GL023851>, 2005.
- Cadeddu, M. P.: Microwave Radiometer – 3-Channel (MWR3C) Instrument Handbook, U.S. Department of Energy, Office of Science, <https://doi.org/10.2172/1039668>, 2021.
- Cadeddu, M. P., Ghate, V. P., Turner, D. D., and Surlleta, T. E.: Boundary layer moisture variability at the Atmospheric Radiation Measurement (ARM) Eastern North Atlantic observatory during marine conditions, *Atmos. Chem. Phys.*, 23, 3453–3470, <https://doi.org/10.5194/acp-23-3453-2023>, 2023.
- Chiu, J. C., Marshak, A., Knyazikhin, Y., Wiscombe, W., Barker, H., Barnard, J. C., and Luo, Y.: Remote sensing of cloud properties using ground-based measurements of zenith radiance, *J. Geophys. Res.*, 111, D16201, <https://doi.org/10.1029/2005JD006843>, 2006.
- Chiu, J. C., Huang, C., Marshak, A., Slutsker, I., Giles, D. M., Holben, B. N., Knyazikhin, Y., and Wiscombe, W. J.: Cloud optical depth retrievals from the Aerosol Robotic Network (AERONET) cloud mode observations, *J. Geophys. Res.*, 115, D14202, <https://doi.org/10.1029/2009JD013121>, 2010.
- Chiu, J. C., Marshak, A., Huang, C.-H., Várnai, T., Hogan, R. J., Giles, D. M., Holben, B. N., O’Connor, E. J., Knyazikhin, Y., and Wiscombe, W. J.: Cloud droplet size and liquid water path retrievals from zenith radiance measurements: examples from the Atmospheric Radiation Measurement Program and the Aerosol Robotic Network, *Atmos. Chem. Phys.*, 12, 10313–10329, <https://doi.org/10.5194/acp-12-10313-2012>, 2012.
- Clothiaux, E. E., Ackerman, T. P., Mace, G. G., Moran, K. P., Marchand, R. T., Miller, M. A., and Martner, B. E.: Objective determination of cloud heights and radar reflectivities using a combination of active remote sensors at the ARM CART sites, *J. Appl. Meteorol.*, 39, 645–665, 2000.
- Deng, M., Giangrande, S. E., Jensen, M. P., Johnson, K., Williams, C. R., Comstock, J. M., Feng, Y.-C., Matthews, A., Lindenmaier, I. A., Wendler, T. G., Rocque, M., Zhou, A., Zhu, Z., Luke, E., and Wang, D.: Wet-radiance attenuation in ARM cloud radars and its utilization in radar calibration using disdrometer measurements, *Atmos. Meas. Tech.*, 18, 1641–1657, <https://doi.org/10.5194/amt-18-1641-2025>, 2025.
- Dunn, M., Johnson, K. L., and Jensen, M. P.: The Microbase Value-Added Product: A Baseline Retrieval of Cloud Microphysical Properties, U.S. Department of Energy, Office of Science, DOE/SC-ARM/TR-095, 2011.
- Fairless, T., Jensen, M., Zhou, A., and Giangrande, S. E.: Interpolated Sounding and Gridded Sounding Value-Added Products, U.S. Department of Energy, Office of Science, <https://doi.org/10.2172/1248938>, 2021.
- Frisch, A. S., Fairall, C. W., and Snider, J. B.: Measurement of stratus cloud and drizzle parameters in ASTEX with a K α -band Doppler radar and a microwave radiometer, *J. Atmos. Sci.*, 52, 2788–2799, 1995.
- Geerts, B., Giangrande, S. E., McFarquhar, G. M., Xue, L., Abel, S. J., Comstock, J. M., Crewell, S., DeMott, P. J., Ebell, K., Field, P., Hill, T. C. J., Hunzinger, A., Jensen, M. P., Johnson, K. L., Juliano, T. W., Kollias, P., Kosovic, B., Lackner, C., Luke, E., Lüpfkes, C., Matthews, A. A., Neggiers, R., Ovchinnikov, M., Powers, H., Shupe, M. D., Spengler, T., Swanson, B. E., Tjernström, M., Theisen, A. K., Wales, N. A., Wang, Y., Wendisch, M., and Wu, P.: The COMBLE Campaign: A Study of Marine Boundary Layer Clouds in Arctic Cold-Air Outbreaks, *B. Am. Meteorol. Soc.*, 103, E1371–E1389, <https://doi.org/10.1175/BAMS-D-21-0044.1>, 2022.
- Ghate, V. P., Cadeddu, M. P., Zheng, X., and O’Connor, E.: Turbulence in the Marine Boundary Layer and Air Motions below Stratocumulus Clouds at the ARM Eastern North Atlantic Site, *J. Appl. Meteorol. Clim.*, 60, 1495–1510, <https://doi.org/10.1175/JAMC-D-21-0087.1>, 2021.
- Giangrande, S. E., Wang, D., Bartholomew, M. J., Jensen, M. P., Mechem, D. B., Hardin, J. C., and Wood, R.: Midlatitude oceanic cloud and precipitation properties as sampled by the ARM Eastern North Atlantic Observatory, *J. Geophys. Res.-Atmos.*, 124, 4741–4760, <https://doi.org/10.1029/2018JD029667>, 2019.

- Gregory, L.: Cimel Sunphotometer (CSPHOT) Handbook, U.S. Department of Energy, Office of Science, <https://doi.org/10.2172/1020262>, 2011.
- Hartmann, D. L., Ockert-Bell, M. E., and Michelsen, M. L.: The effect of cloud type on Earth's energy balance: Global analysis, *J. Climate*, 5, 1281–1304, [https://doi.org/10.1175/1520-0442\(1992\)005%3C1281:TEOCTO%3E2.0.CO;2](https://doi.org/10.1175/1520-0442(1992)005%3C1281:TEOCTO%3E2.0.CO;2), 1992.
- Holben, B. N., Eck, T. F., Slutsker, I., Tanré, D., Buis, J. P., Setzer, A., Vermote, E., Reagan, J. A., Kaufman, Y. J., Nakajima, T., Lavenu, F., Jankowiak, I., and Smirnov, A.: AERONET: A federated instrument network and data archive for aerosol characterization, *Remote Sens. Environ.*, 66, 1–16, 1998.
- Houze Jr., R. A.: Orographic effects on precipitating clouds, *Rev. Geophys.*, 50, RG1001, <https://doi.org/10.1029/2011RG000365>, 2012.
- Huang, D., Zhao, C., Dunn, M., Dong, X., Mace, G. G., Jensen, M. P., Xie, S., and Liu, Y.: An intercomparison of radar-based liquid cloud microphysics retrievals and implications for model evaluation studies, *Atmos. Meas. Tech.*, 5, 1409–1424, <https://doi.org/10.5194/amt-5-1409-2012>, 2012.
- IPCC: Climate change 2013: The physical science basis: Contribution of Working Group to the Fifth Assessment Report of the Intergovernmental Panel on Climate Change, Cambridge University Press, New York, <https://doi.org/10.1017/cbo9781107415324>, 2013.
- Jeong, J.-H., Witte, M. K., Glenn, I. B., Smalley, M., Lebsack, M. D., Lamer, K., and Zhu, Z.: Distinct dynamical and structural properties of marine stratocumulus and shallow cumulus clouds in the Eastern North Atlantic, *J. Geophys. Res.-Atmos.*, 127, e2022JD037021, <https://doi.org/10.1029/2022JD037021>, 2022.
- Klein, S. A.: Synoptic variability of low cloud properties and meteorological parameters in the subtropical trade wind boundary layer, *J. Climate*, 10, 2018–2039, [https://doi.org/10.1175/1520-0442\(1997\)010<2018:SVOLCP>2.0.CO;2](https://doi.org/10.1175/1520-0442(1997)010<2018:SVOLCP>2.0.CO;2), 1997.
- Klein, S. A. and Hartmann, D. L.: The seasonal cycle of low stratiform clouds, *J. Climate*, 6, 1587–1606, [https://doi.org/10.1175/1520-0442\(1993\)006<1587:TSCOLS>2.0.CO;2](https://doi.org/10.1175/1520-0442(1993)006<1587:TSCOLS>2.0.CO;2), 1993.
- Kollias, P. and Albrecht, B.: The Turbulence Structure in a Continental Stratocumulus Cloud from Millimeter-Wavelength Radar Observations, *J. Atmos. Sci.*, 57, 2417–2434, [https://doi.org/10.1175/1520-0469\(2000\)057<2417:TTSIAC>2.0.CO;2](https://doi.org/10.1175/1520-0469(2000)057<2417:TTSIAC>2.0.CO;2), 2000.
- Kollias, P., Bharadwaj, N.; Clothiaux, E. E.; Lamer, K.; Oue, M.; Hardin, J.; Isom, B.; Lindenmaier, I.; Matthews, A.; Luke, E. P.; Giangrande, S. E.; Johnson, K.; Collis, S.; Comstock, J., and Mather, J. H.: The ARM Radar Network: At the Leading Edge of Cloud and Precipitation Observations, *B. Am. Meteorol. Soc.*, 101, E588–E607, <https://doi.org/10.1175/BAMS-D-18-0288.1>, 2020.
- Lebsack, M. D., L'Ecuyer, T. S., and Stephens, G. L.: Detecting the ratio of rain and cloud water in low-latitude shallow marine clouds, *J. Appl. Meteorol. Clim.*, 50, 419–432, <https://doi.org/10.1175/2010JAMC2494.1>, 2011.
- Liao, L. and Sassen, K.: Investigation of relationships between Ka-band radar reflectivity and ice and liquid water contents, *Atmos. Res.*, 34, 231–248, 1994.
- Long, C. N., Ackerman, T. P., Gaustad, K. L., and Cole, J. N. S.: Estimation of fractional sky cover from broadband shortwave radiometer measurements, *J. Geophys. Res.-Atmos.*, 111, D11204, <https://doi.org/10.1029/2005JD006475>, 2006.
- Lubin, D., Zhang, D., Silber, I., Scott, R. C., Kalogeras, P., Battaglia, A., Bromwich, D. H., Cadeddu, M., Eloranta, E., Fridlind, A., Frossard, A., Hines, K. M., Kneifel, S., Leaitch, W. R., Lin, W., Nicolas, J., Powers, H., Quinn, P. K., Rowe, P., Russell, L. M., Sharma, S., Verlinde, J., and Vogelmann, A. M.: AWARE: The Atmospheric Radiation Measurement (ARM) West Antarctic Radiation Experiment, *B. Am. Meteorol. Soc.*, 101, E1069–E1091, <https://doi.org/10.1175/BAMS-D-18-0278.1>, 2020.
- Mann, H. B. and Whitney, D. R.: On a Test of Whether one of Two Random Variables is Stochastically Larger than the Other, *Ann. Math. Statist.*, 18, 50–60, <https://doi.org/10.1214/aoms/1177730491>, 1947.
- Marshak, A., Knyazikhin, Y., Evans, K. D., and Wiscombe, W. J.: The “RED versus NIR” Plane to Retrieve Broken-Cloud Optical Depth from Ground-Based Measurements, *J. Atmos. Sci.*, 61, 1911–1925, [https://doi.org/10.1175/1520-0469\(2004\)061<1911:TRVNPT>2.0.CO;2](https://doi.org/10.1175/1520-0469(2004)061<1911:TRVNPT>2.0.CO;2), 2004.
- Masuda, R., Iwabuchi, H., Schmidt, K. S., Damiani, A., and Kudo, R.: Retrieval of Cloud Optical Thickness from Sky-View Camera Images using a Deep Convolutional Neural Network based on Three-Dimensional Radiative Transfer, *Remote Sens.*, 11, 1962, <https://doi.org/10.3390/rs11171962>, 2019.
- Mather, J. H. and Voyles, J. W.: The Arm Climate Research Facility: A Review of Structure and Capabilities, *B. Am. Meteorol. Soc.*, 94, 377–392, <https://doi.org/10.1175/BAMS-D-11-00218.1>, 2013.
- McComiskey, A., Feingold, G., Frisch, A. S., Turner, D. D., Miller, M. A., Chiu, J. C., Min, Q., and Ogren, J. A.: An assessment of aerosol-cloud interactions in marine stratus clouds based on surface remote sensing, *J. Geophys. Res.*, 114, D09203, <https://doi.org/10.1029/2008JD011006>, 2009.
- McFarquhar, G. M., Bretherton, C., Marchand, R., Protat, A., DeMott, P. J., Alexander, S. P., Roberts, G. C., Twohy, C. H., Toohey, D., Siems, S., Huang, Y., Wood, R., Rauber, R. M., Lasher-Trapp, S., Jensen, J., Stith, J., Mace, J., Um, J., Järvinen, E., Schnaiter, M., Gettelman, A., Sanchez, K. J., McCluskey, C. S., Russell, L. M., McCoy, I. L., Atlas, R., Bardeen, C. G., Moore, K. A., Hill, T. C. J., Humphries, R. S., Keywood, M. D., Ristovski, Z., Cravigan, L., Schofield, R., Fairall, C., Mallet, M. D., Kreidenweis, S. M., Rainwater, B., D'Alessandro, J., Wang, Y., Wu, W., Saliba, G., Levin, E. J. T., Ding, S., Lang, F., Truong, S. C. H., Wolff, C., Haggerty, J., Harvey, M. J., Klekociuk, A. R., and McDonald, A.: Observations of Clouds, Aerosols, Precipitation, and Surface Radiation over the Southern Ocean: An Overview of CAPRICORN, MARCUS, MICRE, and SOCRATES, *B. Am. Meteorol. Soc.*, 102, E894–E928, <https://doi.org/10.1175/BAMS-D-20-0132.1>, 2021.
- Mechem, D. B., Kogan, Y. L., and Schultz, D. M.: Large-Eddy Observation of Post-Cold-Frontal Continental Stratocumulus, *J. Atmos. Sci.*, 67, 3368–3383, <https://doi.org/10.1175/2010JAS3389.1>, 2010.
- Mechem, D. B., Wittman, C. S., Miller, M. A., Yuter, S. E., and de Szoeke, S. P.: Joint Synoptic and Cloud Variability over the Northeast Atlantic near the Azores, *J. Appl. Meteorol. Clim.*, 57, 1273–1290, <https://doi.org/10.1175/JAMC-D-17-0211.1>, 2018.

- Miller, M. A., Nitschke, K., Ackerman, T. P., Ferrell, W. R., Hickmon, N., and Ivey, M.: The ARM Mobile Facilities, *Meteor. Monogr.*, 57, 9.1–9.15, <https://doi.org/10.1175/AMSMONOGRAPHS-D-15-0051.1>, 2016.
- Min, Q. and Harrison, L. C.: Cloud properties derived from surface MFRSR measurements and comparison with GOES results at the ARM SGP site, *Geophys. Res. Lett.*, 23, 1641–1644, 1996.
- Min, Q., Duan, M., and Marchand, R.: Validation of surface retrieved cloud optical properties with in situ measurements at the Atmospheric Radiation Measurement Program (ARM) South Great Plains site, *J. Geophys. Res.*, 108, 4547, <https://doi.org/10.1029/2003JD003385>, 2003.
- Minnis, P., Sun-Mack, S., Young, D. F., Heck, P. W., Garber, D. P., Chen, Y., Spangenberg, D. A., Arduini, R. F., Trepte, Q. Z., Smith, W. L., Ayers, J. K., Gibson, S. C., Miller, W. F., Hong, G., Chakrapani, V., Takano, Y., Liou, K. N., Xie, Y., and Yang, P.: CERES Edition-2 Cloud Property Retrievals Using TRMM VIRS and Terra and Aqua MODIS Data – Part I: Algorithms, *IEEE T. Geosci. Remote*, 49, 4374–4400, <https://doi.org/10.1109/TGRS.2011.2144601>, 2011.
- Morris, V. R.: Microwave Radiometer (MWR) Handbook, U.S. Department of Energy, Office of Science, DOE/SC-ARM-TR-016, <https://doi.org/10.2172/1020715>, 2019.
- Pörtge, V., Kölling, T., Weber, A., Volkmer, L., Emde, C., Zinner, T., Forster, L., and Mayer, B.: High-spatial-resolution retrieval of cloud droplet size distribution from polarized observations of the cloudbow, *Atmos. Meas. Tech.*, 16, 645–667, <https://doi.org/10.5194/amt-16-645-2023>, 2023.
- Rémillard, J., Kollias, P., Luke, E., and Wood, R.: Marine Boundary Layer Cloud Observations in the Azores, *J. Climate*, 25, 7381–7398, <https://doi.org/10.1175/JCLI-D-11-00610.1>, 2012.
- Rosenfeld, D. and Gutman, G.: Retrieving microphysical properties near the tops of potential rain clouds by multispectral analysis of AVHRR data, *Atmos. Res.*, 34, 259–283, 1994.
- Rosenfeld, D., Wang, H., and Rasch, P. J.: The roles of cloud drop effective radius and LWP in determining rain properties in marine stratocumulus, *Geophys. Res. Lett.*, 39, L13801, <https://doi.org/10.1029/2012GL052028>, 2012.
- Schaaf, C. B., Gao, F., Strahler, A. H., Lucht, W., Li, X. W., Tsang, T., Strugnell, N. C., Zhang, X. Y., Jin, Y. F., Muller, J. P., Lewis, P., Barnsley, M., Hobson, P., Disney, M., Roberts, G., Dunderdale, M., Doll, C., d’Entremont, R. P., Hu, B. X., Liang, S. L., Privette, J. L., and Roy, D.: First operational BRDF, albedo nadir reflectance products from MODIS, *Remote Sens. Environ.*, 83, 135–148, 2002.
- Sherwood, S. C., Webb, M. J., Annan, J. D., Armour, K. C., Forster, P. M., Hargreaves, J. C., Hegerl, G., Klein, S. A., Marvel, K. D., Rohling, E. J., Watanabe, M., Andrews, T., Braconnot, P., Bretherton, C. S., Foster, G. L., Hausfather, Z., von der Heydt, A. S., Knutti, R., Mauritsen, T., Norris, J. R., Proistosescu, C., Rugenstein, M., Schmidt, G. A., Tokarska, K. B., and Zelinka, M. D.: An assessment of Earth’s climate sensitivity using multiple lines of evidence, *Rev. Geophys.*, 58, e2019RG000678, <https://doi.org/10.1029/2019RG000678>, 2020.
- Sisterson, D. L., Peppler, R. A., Cress, T. S., Lamb, P. J., and Turner, D. D.: The ARM Southern Great Plains (SGP) Site, *Meteor. Monogr.*, 57, 6.1–6.14, <https://doi.org/10.1175/AMSMONOGRAPHS-D-16-0004.1>, 2016.
- Stamnes, K., Tsay, S.-C., Wiscombe, W. J., and Jayaweera, K.: Numerically stable algorithm for discrete-ordinate-method radiative transfer in multiple scattering and emitting layered media, *Appl. Opt.*, 27, 2502–2512, 1988.
- Stephens, G. L.: Radiation profiles in extended water clouds I: Theory, *J. Atmos. Sci.*, 35, 2111–2122, [https://doi.org/10.1175/1520-0469\(1978\)035<2111:RPIEWC>2.0.CO;2](https://doi.org/10.1175/1520-0469(1978)035<2111:RPIEWC>2.0.CO;2), 1978.
- Turner, D., Lo, C., and Min, Q.: Cloud Optical Properties from the MultiFilter Shadowband Radiometer (MFRSRCLDOD): An ARM Value-Added Product, U.S. Department of Energy, Office of Science, DOE/SC-ARM/TR-047, 2004.
- Turner, D. D.: Improved ground-based liquid water path retrievals using a combined infrared and microwave approach, *J. Geophys. Res.*, 112, D15204, <https://doi.org/10.1029/2007JD008530>, 2007.
- Turner, D. D. and Blumberg, W. G.: Improvements to the AERIoe thermodynamic profile retrieval algorithm, *IEEE J. Sel. Top. Appl. Earth Obs. Remote Sens.*, 12, 1339–1354, <https://doi.org/10.1109/JSTARS.2018.2874968>, 2019.
- Turner, D. D. and Löhnert, U.: Ground-based temperature and humidity profiling: combining active and passive remote sensors, *Atmos. Meas. Tech.*, 14, 3033–3048, <https://doi.org/10.5194/amt-14-3033-2021>, 2021.
- Turner, D. D. and Loehnert, U.: Information content and uncertainties in thermodynamic profiles and liquid cloud properties retrieved from the ground-based Atmospheric Emitted Radiance Interferometer (AERI), *J. Appl. Meteorol. Clim.*, 53, 752–771, <https://doi.org/10.1175/JAMC-D-13-0126.1>, 2014.
- Turner, D. D., Clough, S. A., Liljegren, J. C., Clothiaux, E. E., Cady-Pereira, K., and Gaustad, K. L.: Retrieving liquid water path and precipitable water vapor from Atmospheric Radiation Measurement (ARM) microwave radiometers, *IEEE T. Geosci. Remote Sens.*, 45, 3680–3690, <https://doi.org/10.1109/TGRS.2007.903703>, 2007.
- Wang, J., Wood, R., Jensen, M. P., Chiu, J. C., Liu, Y., Lamer, K., Desai, N., Giangrande, S. E., Knopf, D. A., Kollias, P., Laskin, A., Liu, X., Lu, C., Mechem, D., Mei, F., Starzec, M., Tomlinson, J., Wang, Y., Yum, S. S., Zheng, G., Aiken, A. C., Azevedo, E. B., Blanchard, Y., China, S., Dong, X., Gallo, F., Gao, S., Ghate, V. P., Glienke, S., Goldberger, L., Hardin, J. C., Kuang, C., Luke, E. P., Matthews, A. A., Miller, M. A., Moffet, R., Pekour, M., Schmid, B., Sedlacek, A. J., Shaw, R. A., Shilling, J. E., Sullivan, A., Suski, K., Veghte, D. P., Weber, R., Wyant, M., Yeom, J., Zawadowicz, M., and Zhang, Z.: Aerosol and Cloud Experiments in the Eastern North Atlantic (ACE-ENA), *Bull. Amer. Meteor. Soc.*, 103, E619–E641, <https://doi.org/10.1175/BAMS-D-19-0220.1>, 2022.
- Williams, C. R., Johnson, K. L., Giangrande, S. E., Hardin, J. C., Öktem, R., and Romps, D. M.: Identifying insects, clouds, and precipitation using vertically pointing polarimetric radar Doppler velocity spectra, *Atmos. Meas. Tech.*, 14, 4425–4444, <https://doi.org/10.5194/amt-14-4425-2021>, 2021.
- Wood, R. and Harmann, D. L.: Spatial variability of liquid water path in marine low cloud: The importance of mesoscale cellular convection, *J. Climate*, 19, 1748–1764, 2006.
- Wood, R., Wyant, M., Bretherton, C. S., Rémillard, J., Kollias, P., Fletcher, J., Stemmler, J., de Szoeko, S., Yuter, S., Miller,

- M., Mechem, D., Tselioudis, G., Chiu, J. C., Mann, J. A. L., O'Connor, E. J., Hogan, R. J., Dong, X., Miller, M., Ghate, V., Jefferson, A., Min, Q., Minnis, P., Palikonda, R., Albrecht, B., Luke, E., Hannay, C., and Lin, Y.: Clouds, Aerosols, and Precipitation in the Marine Boundary Layer: An Arm Mobile Facility Deployment, *B. Am. Meteorol. Soc.*, 96, 419–440, <https://doi.org/10.1175/BAMS-D-13-00180.1>, 2015.
- Yang, F., Luke, E. P., Kollias, P., Kostinski, A. B., and Vogelmann, A. M.: Scaling of drizzle virga depth with cloud thickness for marine stratocumulus clouds, *Geophys. Res. Lett.*, 45, 3746–3753, <https://doi.org/10.1029/2018GL077145>, 2018.
- Zhao C., Xie, S., Klein, S. A., Protat, A., Shupe, M. D., McFarlane, S. A. Comstock, J. M., Delanoë, J., Deng, M., Dunn, M., Hogan, R. J., Huang, D., Jensen, M. P., Mace, G. G., McCoy, R., O'Connor, E. J., Turner, D. D., and Wang, Z.: Toward understanding of differences in current cloud retrievals of ARM ground-based measurements, *J. Geophys. Res.*, 117, D10206, <https://doi.org/10.1029/2011JD016792>, 2012.
- Zhao, C., Xie, S., Chen, X., Jensen, M. P., and Dunn, M.: Quantifying uncertainties of cloud microphysical property retrievals with a perturbation method, *J. Geophys. Res.-Atmos.*, 119, 5375–5385, <https://doi.org/10.1002/2013JD021112>, 2014.
- Zhu, Z., Kollias, P., Luke, E., and Yang, F.: New insights on the prevalence of drizzle in marine stratocumulus clouds based on a machine learning algorithm applied to radar Doppler spectra, *Atmos. Chem. Phys.*, 22, 7405–7416, <https://doi.org/10.5194/acp-22-7405-2022>, 2022.
- Zhu, Z., Yang, F., Kollias, P., Lamer, K., Luke, E., Mead, J. B., Sua, Y. M., Vogelmann, A. M., and McComiskey, A.: Peering into Cloud Physics Using Ultra-Fine-Resolution Radar and Lidar Systems, *B. Am. Meteorol. Soc.*, 105, E2010–E2025, <https://doi.org/10.1175/BAMS-D-23-0032.1>, 2024.